AMERICAN SOCIETY FOR MICROBIOLOGY | Infection and Immunity

Persisting *Rickettsia typhi* Causes Fatal Central Nervous System Inflammation

Anke Osterloh,[a] Stefanie Papp,[a] Kristin Moderzynski,[a] Svenja Kuehl,[a] Ulricke Richardt,[a] Bernhard Fleischer[b]

Department of Immunology, Bernhard Nocht Institute for Tropical Medicine, Hamburg, Germany[a]; Institute for Immunology, University Medical Center Hamburg-Eppendorf, Hamburg, Germany[b]

Rickettsioses are emerging febrile diseases caused by obligate intracellular bacteria belonging to the family *Rickettsiaceae*. *Rickettsia typhi* belongs to the typhus group (TG) of this family and is the causative agent of endemic typhus, a disease that can be fatal. In the present study, we analyzed the course of *R. typhi* infection in C57BL/6 RAG1$^{-/-}$ mice. Although these mice lack adaptive immunity, they developed only mild and temporary symptoms of disease and survived *R. typhi* infection for a long period of time. To our surprise, 3 to 4 months after infection, C57BL/6 RAG1$^{-/-}$ mice suddenly developed lethal neurological disorders. Analysis of these mice at the time of death revealed high bacterial loads, predominantly in the brain. This was accompanied by a massive expansion of microglia and by neuronal cell death. Furthermore, high numbers of infiltrating CD11b^{+} macrophages were detectable in the brain. In contrast to the microglia, these cells harbored *R. typhi* and showed an inflammatory phenotype, as indicated by inducible nitric oxide synthase (iNOS) expression, which was not observed in the periphery. Having shown that *R. typhi* persists in immunocompromised mice, we finally asked whether the bacteria are also able to persist in resistant C57BL/6 and BALB/c wild-type mice. Indeed, *R. typhi* could be recultivated from lung, spleen, and brain tissues from both strains even up to 1 year after infection. This is the first report demonstrating persistence and reappearance of *R. typhi*, mainly restricted to the central nervous system in immunocompromised mice.

Rickettsioses are arthropod-borne neglected and emerging febrile diseases that are caused by small obligate intracellular bacteria (family *Rickettsiaceae*). Based on phylogenetic analyses, the family *Rickettsiaceae* is subdivided into three major groups, the spotted fever group (SFG), the typhus group (TG), and the scrub typhus group (1, 2). The majority of rickettsiae identified so far are SFG bacteria. Prominent members of this group are *Rickettsia rickettsii* and *Rickettsia conorii*, the causative agents of Rocky Mountain spotted fever (RMSF) and Mediterranean spotted fever (MSF). *Orientia* (*Rickettsia*) *tsutsugamushi* is the only member of the scrub typhus group, while *Rickettsia prowazekii* and *Rickettsia typhi* represent the two members of TG rickettsiae (3, 4).

R. prowazekii and *R. typhi* are the causative agents of epidemic and endemic typhus, respectively. Endemic typhus is distributed worldwide and highly prevalent in low-income countries in Africa (5) and Asia (6–9). The disease primarily occurs in ports and coastal towns where rodents such as rats and mice that serve as natural hosts of *R. typhi* are common. The bacteria are transmitted from these animals to humans by fleas (10, 11). Epidemic and endemic typhus appear with similar symptoms. After 10 to 14 days of latency, the disease starts with the sudden onset of high fever that lasts for several days and is accompanied by headache, myalgia and joint pain, and nausea and vomiting. In addition, neurological symptoms, such as confusion and stupor, are common (12). Because endothelial cells are the main target cells of rickettsiae, many patients develop a characteristic hemorrhagic rash due to local blood vessel damage and inflammation (2). In severe cases, systemic infection leads to multiorgan pathology and potentially fatal complications, including pneumonia, myocarditis, and nephritis, as well as encephalitis or meningitis (12, 13). The course of disease of endemic typhus is generally milder than that of epidemic typhus. The lethality of *R. typhi* infection is estimated to be <5% (14, 15), while the lethality of *R. prowazekii* infection is much higher (20 to 30%) (13, 15, 16) if untreated with an effective antibiotic, such as a tetracycline or chloramphenicol.

In the past years, mouse models for rickettsial infections employing different mouse strains have been established. Among these, BALB/c and C57BL/6 mice were found to be resistant to rickettsial infections (17–21), while C3H/HeN mice have been described as being susceptible (17, 21). The latter have been intensively investigated with regard to immune response against SFG rickettsiae. It has been shown that cytotoxic CD8^{+} T cells, in addition to gamma interferon (IFN-γ), are essential for protection against SFG rickettsiae in these animals (22–25). In contrast to C3H/HeN mice, C57BL/6 mice can survive SFG rickettsial infections even in the absence of adaptive immunity. C57BL/6 RAG1$^{-/-}$ mice, which lack both mature T and B cells (26), clear and survive the infection with *R. conorii* at least until day 20 (27), demonstrating that C57BL/6 mice mount an efficient innate immune response that is capable of controlling the bacteria. However, little is known about the course of infection and immune response against TG rickettsiae.

In the present study, we infected C57BL/6 RAG1$^{-/-}$ mice with

Received 11 January 2016 **Returned for modification** 5 February 2016
Accepted 6 March 2016

Accepted manuscript posted online 14 March 2016

Citation Osterloh A, Papp S, Moderzynski K, Kuehl S, Richardt U, Fleischer B. 2016. Persisting *Rickettsia typhi* causes fatal central nervous system inflammation. Infect Immun 84:1615–1632. doi:10.1128/IAI.00034-16.

Editor: C. R. Roy

Address correspondence to Anke Osterloh, osterloh@bni-hamburg.de.

A.O. and S.P. contributed equally to this work.

Supplemental material for this article may be found at http://dx.doi.org/10.1128/IAI.00034-16.

R. typhi, a representative of the TG rickettsiae. Similar to the findings with SFG rickettsiae mentioned above, we observed that T and B cell-deficient mice were mainly asymptomatic in the initial phase and survived the infection independent of the route of infection for at least as long as described for *R. conorii* infection. To our surprise, however, all mice without exception suddenly developed lethal neurological disorders 3 to 4 months after *R. typhi* infection. High numbers of *R. typhi* were then detectable in the brain of the animals, while peripheral organs were hardly affected. In the brain as well as in the spinal cord of these mice, we observed massive expansion of microglia, the resident macrophages of the central nervous system (CNS), which was associated with neuronal cell death. *R. typhi* was detectable in these areas of microglial accumulation. Flow cytometric analysis, however, revealed that the microglia did not harbor *R. typhi*. Furthermore, they did not express inducible nitric oxide synthase (iNOS), which is responsible for the synthesis of bactericidal nitric oxide (NO) (28). Thus, microglia did not exert inflammatory activity that is characteristic of classically activated macrophages. In addition to microglial expansion, high numbers of infiltrating macrophages were observed in the brain of infected animals. In contrast to microglia, these cells expressed iNOS. Furthermore, *R. typhi* particles were detectable within these infiltrating macrophages but not in either endothelial or neuronal cells. Despite NO production, the particles appeared intact, indicating bacterial survival and replication. Finally, having observed that *R. typhi* persists in C57BL/6 RAG1$^{-/-}$ mice, we asked whether the bacteria might also persist in wild-type mice, and we demonstrate that *R. typhi* can be recultivated from resistant immunocompetent C57BL/6 mice, as well as BALB/c wild-type mice, even up to 1 year postinfection.

Collectively, our data demonstrate for the first time persistence of *R. typhi* in wild-type mice and reappearance of the bacteria selectively in the CNS of immunocompromised mice, causing lethal CNS inflammation.

MATERIALS AND METHODS

Mice. C57BL/6, BALB/c, and C57BL/6 RAG1$^{-/-}$ mice were bred in the animal facilities of the Bernhard Nocht Institute for Tropical Medicine and housed in a biosafety level 3 facility for experimentation. The facilities are registered by the Public Health Authorities (Amt für Gesundheit und Verbraucherschutz, Hamburg, Germany). All experiments and procedures were approved by the Public Health Authorities (Amt für Gesundheit und Verbraucherschutz, Hamburg, Germany; no. 61/12 and no. 88/13) and performed according to the requirements of the German Animal Welfare Act.

Infection of mice. *R. typhi* stocks were thawed and washed in phosphate-buffered saline (PBS) as described below. Inocula of 2×10^6 spot-forming units (SFU) were administered in 50 μl of PBS subcutaneously (s.c.) into the base of the tail or in 100 μl PBS intravenously (i.v.) into the tail vein. Serum samples were obtained by submandibular bleeding.

Culture and purification of *R. typhi*. *R. typhi* (strain Wilmington) was cultured with L929 mouse fibroblasts (ATCC CCL-1) in RPMI 1640 (PAA Laboratories, Cölbe, Germany) supplemented with 10% fetal calf serum (FCS) (PAA Laboratories), 2 mM L-glutamine (PAA Laboratories), and 10 mM HEPES (PAA Laboratories) without antibiotics (standard culture medium). Amounts of 1×10^7 gamma-irradiated (1,966 rads) L929 cells were seeded in 175-cm^2 culture flasks (Greiner Bio-One, Frickenhausen, Germany). One day later, cells were infected with *R. typhi* and incubated for 5 to 7 days. For the preparation of bacterial stocks, infected L929 cells were resuspended in 1.5 ml PBS. Amounts of 200 μl of silicon carbide particles (60/90 grit; Lortone, Inc., Mukilteo, WA) were added, and cells were vortexed thoroughly for 1 min. The crude lysate was strained through a 2-μm cell strainer (Puradisc 25 2-μm syringe filter; GE Healthcare Life Sciences, Freiburg, Germany). Bacteria were centrifuged at 6,200 × *g* for 5 min at room temperature and frozen in FCS with 7.5% dimethyl sulfoxide (DMSO) in liquid nitrogen in Cryo.S tubes (Greiner Bio-One, Frickenhausen, Germany). Thawed bacterial stocks were centrifuged at 6,200 × *g* for 5 min at room temperature, washed twice with PBS, and analyzed for bacterial content by quantitative real-time PCR (qPCR) and immunofocus assay to determine the SFU counts.

DNA preparation from purified bacteria, cell cultures, and organs. DNA was prepared from purified bacteria, cell cultures, and organs by using the QIAamp DNA minikit (Qiagen, Hilden, Germany). An amount of 10 mg of tissue was homogenized in 500 μl of PBS in Precellys ceramic kit tubes (Peqlab, Erlangen, Germany) two times at 6,000 rpm for 45 s with a 60-s break in a Precellys 24 homogenizer (Peqlab, Erlangen, Germany). Eighty microliters of tissue homogenate or up to 1×10^6 cells was used for DNA preparation according to the manufacturer's instructions.

qPCR. Quantification of *R. typhi* was performed by amplification of a 137-bp fragment of the *prsA* gene (locus tag RT_RS02795). The *prsA* forward primer, 5′-ACA GCT TCA AAT GGT GGG GT-3′, and reverse primer, 5′-TGC CAG CCG AAA TCT GTT TTG-3′, were used in a standard SYBR green qPCR. A standard template plasmid (pCR2.1-PrsA) containing the same *prsA* DNA fragment was used at calculated copy numbers for quantification. Reactions were performed in a Rotor Gene 6000 (Qiagen, Hilden, Germany) in a total volume of 10 μl comprising 1.5 mM $MgCl_2$, 0.175 mM deoxynucleoside triphosphates (dNTPs), 100 nM primers, 0.05× SYBR green I nucleic acid gel stain (Sigma Life Sciences, Deisenhofen, Germany), and 0.25 U HotStar *Taq* DNA polymerase (Qiagen, Hilden, Germany) under the following conditions: 15 min preheating at 95°C, followed by 40 cycles of denaturing (94°C for 20 s), primer annealing (53°C for 30 s), and elongation (72°C for 20 s).

Immunofocus assay. Amounts of 1.8×10^5 gamma-irradiated L929 (1,966 rads) cells were seeded into 24-well plates. Cells were incubated with serial dilutions of either purified thawed bacteria or freshly prepared lysates from organs of *R. typhi*-infected mice overnight at 37°C in standard culture medium. Lysates from mouse organs were prepared as follows: organs were homogenized and strained through a 70-μm cell strainer (BD Biosciences, Heidelberg, Germany). Cells were centrifuged at 272 × *g* for 5 min. Cell pellets were resuspended in 100 μl (lung and spleen) or 500 μl (brain) standard medium. Amounts of 200 μl of silicon carbide particles (60/90 grit; Lortone, Inc., Mukilteo, WA) were added, and cell lysis was achieved by vortexing two times for 1 min. The supernatant was strained through a 2-μm cell strainer (Puradisc 25 2-μm syringe filter; GE Healthcare Life Sciences, Freiburg, Germany). The flow-through was added directly to the L929 cell culture in serial dilutions in a total volume of 200 μl of standard medium. The medium was exchanged on the following day against semisolid standard culture medium containing approximately 1% methyl cellulose. Cells were further incubated for 8 to 10 days. The following steps were performed at room temperature (RT). Cells were washed in PBS and fixed in PBS–4% formaldehyde–0.1% Triton X-100 (Sigma-Aldrich, Deisenhofen, Germany) for 20 min, followed by permeabilization in PBS–0.5% Triton X-100 for 20 to 60 min. Cells were blocked with 200 μl PBS–10% FCS for 1 h. For detection of *R. typhi*, a monoclonal *R. typhi*-specific antibody (mouse anti-*R. typhi* antibody [clone BNI52]) was added (1 μg/ml in PBS–10% FCS) overnight at 4°C. Cells were washed in H_2O, followed by incubation with goat anti-mouse antibody–horseradish peroxidase (HRP) (Dako, Hamburg, Germany) (1:400 in PBS–10% FCS) for 1 to 2 h in the dark at RT. Finally, cells were washed and *R. typhi* was detected with Immunoblot 3,3′,5,5′-tetramethylbenzidine (TMB) substrate solution (200 μl; Mikrogen, Neuried, Germany). Plates were finally washed in H_2O, dried, and analyzed with a BZ9000 Keyence microscope (Keyence, Neu-Isenburg, Germany).

Reisolation of *R. typhi* from brain and bacterial detection by immunofluorescence staining of L929 cell cultures. The brains of two infected C57BL/6 RAG1$^{-/-}$ mice were taken at the time of death and homogenized in 600 μl of cell culture medium. Amounts of 200 μl of silicon

carbide particles (60/90 grit; Lortone Inc., Mukilteo, WA) were added, and cells were vortexed thoroughly for 1 min. The crude lysate was strained through a 2-μm cell strainer (Puradisc 25 2-μm syringe filter; GE Healthcare Life Sciences, Freiburg, Germany). Amounts of 500 μl of the flowthrough were directly used to inoculate irradiated L929 cells in 25-cm^2 cell culture flasks and 10 ml of cell culture medium. After 5 days of culture, cells were completely infected. Amounts of 50 μl of supernatants of these cells were used to inoculate 1×10^5 irradiated L929 cells seeded into 8-well Permanox chamber slides (Thermo Fisher Scientific, Braunschweig, Germany). After 3 days, cells were fixed with ice-cold acetone-methanol (2:3) for 10 min at −20°C and stained at 4°C. For blocking, PBS with 5% mouse serum was added for 15 min. Afterwards, cells were incubated with patient serum (1:200 in PBS) for 20 min. After washing in PBS, goat anti-human IgG–fluorescein isothiocyanate (FITC) (1:200; Thermo Fisher Scientific, Braunschweig, Germany) was added for 20 min, and thereafter, cells were washed in PBS. Finally, cells were incubated with DAPI (4′,6-diamidino-2-phenylindole) (1:1,000 in PBS; Sigma-Aldrich, Munich, Germany), and FITC–Alexa Fluor 488-conjugated antibody (1:1,000 in PBS; Thermo Fisher Scientific, Braunschweig, Germany) for 20 min, washed, and sealed with PermaFluor (Thermo Fisher Scientific, Braunschweig, Germany).

NK cell depletion. NK cells were depleted by intraperitoneal application of 100 μl of rabbit anti-asialo GM1 antiserum (986-1001; Wako, Neuss, Germany), while control animals received equivalent amounts of naive rabbit serum (R9133; Sigma-Aldrich, Munich, Germany) 1 day prior to *R. typhi* infection. The treatment was repeated every 5 days. The presence or absence of NK cells was controlled by flow cytometric staining of blood samples with phycoerythrin (PE)-labeled anti-NKp46 antibody (1:20) (clone 29A1.4; Biolegend, London, United Kingdom).

Clinical scoring. The state of health was evaluated by a clinical score. The following five parameters were assessed: posture (0, normal; 1, temporarily curved; and 2, curved), fur condition (0, normal; 1, staring around the neck; and 2, overall staring), activity (0, normal; 1, reduced; and 2, strongly reduced), weight loss (0, <10%; 1, 10 to 14%; and 2, >15%), and food and water uptake (0, normal; 1, reduced; and 2, none). Mice were considered healthy with a score <5, moderately ill with a score of 5 to 7, and severely ill with a score of 8 to 10. Mice were sacrificed upon reaching a total score of >8 or showing weight loss of >20%.

Generation of the *R. typhi*-specific anti-*R. typhi* monoclonal antibody clone BNI52. BALB/c mice were immunized intraperitoneally three times at 3-week intervals with 1×10^7 copies of either formalin- or heat-killed (30 min at 56°C) *R. typhi* bacteria. Three days after the final boost, spleen cells were fused with P3/X63-Ag8.653 myeloma cells by standard procedures as previously described (29). Hybridoma supernatants were screened by staining *R. typhi*-infected L929 cells for immunofluorescence microscopy. Positive hybridomas were further subcloned. Finally, the stable anti-*R. typhi* antibody (clone BNI52) was obtained. The antibody (IgG3, kappa) was purified with protein G Sepharose and used unlabeled for further experimentation.

Flow cytometry. The spleen, brain, and spinal cord from naive and infected mice were homogenized. In addition, blood samples were analyzed. Erythrocyte lysis was performed for spleen and blood by incubating the cells in erythrocyte lysis buffer (10 mM Tris, 144 mM NH_4Cl, pH 7.5) for 5 min at RT. Afterwards, cells were washed two times in PBS. Brain and spinal cord cells were strained through a 30-μm CellTrics cell strainer (Partec, Görlitz, Germany) and used directly for staining. Cells were fixed and permeabilized with Cytofix/Cytoperm and Perm/Wash solutions (BD Biosciences, Heidelberg, Germany) according to the manufacturer's protocol. Fc receptors were blocked with 5% Cohn fraction II human IgG (Sigma-Aldrich, Deisenhofen, Germany) in Perm/Wash for 15 min at 4°C, followed by the addition of either mouse anti-*R. typhi* antibody (clone BNI52) or mouse IgG3 isotype (clone B10; SouthernBiotech, Birmingham, AL), each at a concentration of 1 μg/ml in Perm/Wash. Cells were washed in Perm/Wash after 20 min of incubation at 4°C, followed by incubation for 20 min at 4°C with rat anti-mouse IgG3–FITC (1:200 in Perm/Wash) (1100-02; SouthernBiotech, Birmingham, AL). After washing, cells were further stained with rat anti-mouse iNOS antibody–PE (clone CXNFT; eBioscience, Frankfurt, Germany) and rat anti-mouse CD11b antibody–peridinin chlorophyll protein (PerCP)-Cy5.5 (clone M1/70; BD Biosciences, Heidelberg, Germany). To discriminate immune cells in brain and spinal cord, cells were additionally stained with rat anti-mouse CD45 antibody–Alexa Fluor 647 (clone 30-F11; Biolegend, London, United Kingdom). Rat anti-iNOS antibody–PE, rat anti-CD11b antibody–PerCP Cy5.5, and rat anti-mouse CD45 antibody–Alexa Fluor 647 were used at 1:200 dilutions in Perm/Wash solution. After 20 min at 4°C, cells were finally washed and resuspended in PBS–1% paraformaldehyde. Analysis was performed employing a Accuri flow cytometer and (BD Biosciences, Heidelberg, Germany) and FlowJo software (FlowJo LLC, Ashland, OR).

Histological staining. For immunohistochemistry (IHC), tissues from infected mice were fixed in 4% formalin in PBS and embedded in paraffin. Deparaffinization of the sections was performed using standard methods. Sections were first heated at 63°C for 30 min in a heating cabinet, followed by treatment with xylol for 30 min and then ethyl alcohol (EtOH) (3 times with 100% EtOH and 3 times each with 96% EtOH, 80% EtOH, and 70% EtOH). Each step was performed for 3 to 5 min. The slides were finally washed in H_2O. Deparaffinized sections were boiled for 30 min in 10 mM citrate buffer (10 mM sodium citrate, 0.05% Tween 20, pH 6.0) for antigen retrieval. Staining was performed using a Ventana Benchmark XT apparatus (Ventana, Tucson, AZ). Antibodies were diluted in 5% goat serum (Dianova, Hamburg, Germany) in Tris-buffered saline, pH 7.6 (TBS), and 0.1% Triton X-100 in antibody diluent solution (Zytomed, Berlin, Germany). Rabbit anti-mouse CD3 antibody (1:100) (clone SP7; Abcam, Cambridge, MA, USA), rabbit anti-mouse IBA1 antibody (1:300) (019-19741; WAKO, Neuss, Germany), rabbit anti-mouse iNOS antibody (1:75) (ABIN373696; Abcam, Cambridge, MA, USA), rabbit anti-mouse active caspase 3 antibody–Alexa Fluor 835 (1:800) (R&D Systems, Wiesbaden-Nordenstadt, Germany), rat anti-mouse Ly-6G antibody (1:1,000) (clone 1A8; BD Biosciences, Heidelberg, Germany), rat anti-mouse CD31 antibody (1:100) (clone SZ31; Dianova, Hamburg, Germany), and mouse anti-mouse NeuN antibody (1:50) (MAb 377; Millipore, Darmstadt, Germany) were used. *R. typhi* was detected by employing either anti-*R. typhi* antibody (clone BNI52) monoclonal antibody (1 μg/ml) or serum from an *R. typhi* patient (1:100), as indicated in the figure legends. Slides were incubated with primary antibodies for 1 h. Histofine simple stain MAX anti-mouse, anti-human, anti-rabbit, and anti-rat peroxidase-coupled antibodies (Nichirei Biosciences, Tokyo, Japan) were used as secondary antibodies. Detection was performed with the ultraView universal DAB (3,3′-diaminobenzidine) detection kit (Ventana, Tucson, AZ). For immunofluorescent staining, goat anti-human IgG–FITC (1:200) (H10101C; Thermo Fisher Scientific, Braunschweig, Germany), donkey anti-mouse antibody–Alexa Fluor 555 (1:300) (A31570; Thermo Fisher Scientific, Braunschweig, Germany), donkey anti-rabbit antibody–Alexa Fluor 555 (1:300) (A31572; Thermo Fisher Scientific, Braunschweig, Germany), goat anti-rat antibody–Alexa Fluor 568 (1:300) (A11077; Thermo Fisher Scientific, Braunschweig, Germany), and anti-Alexa Fluor 488 FITC-conjugated antibody (1:1,000; Sigma-Aldrich, Munich, Germany) were used as secondary antibodies. Nuclei were stained with DAPI (1:1,000; Sigma-Aldrich, Munich, Germany). Sections were covered with Tissue-Tek embedding medium (Sakura Finetek, Staufen, Germany). Images were taken with a BZ9000 Keyence microscope (Keyence, Neu-Isenburg, Germany).

Quantification of serum GPT. Serum glutamate pyruvate transaminase (GPT) content was quantified with Reflotron GTP (ALT) strips (10745138; Roche Diagnostics, Mannheim, Germany) with a Reflotron plus apparatus (Roche Diagnostics, Mannheim, Germany). The strips were incubated with 32 μl of serum diluted 1:3 in PBS.

Detection of plasma cytokines by bead-based LEGENDplex assay. Plasma cytokines were detected by using the bead-based LEGENDplex assay (Biolegend, London, United Kingdom) according to the manufac-

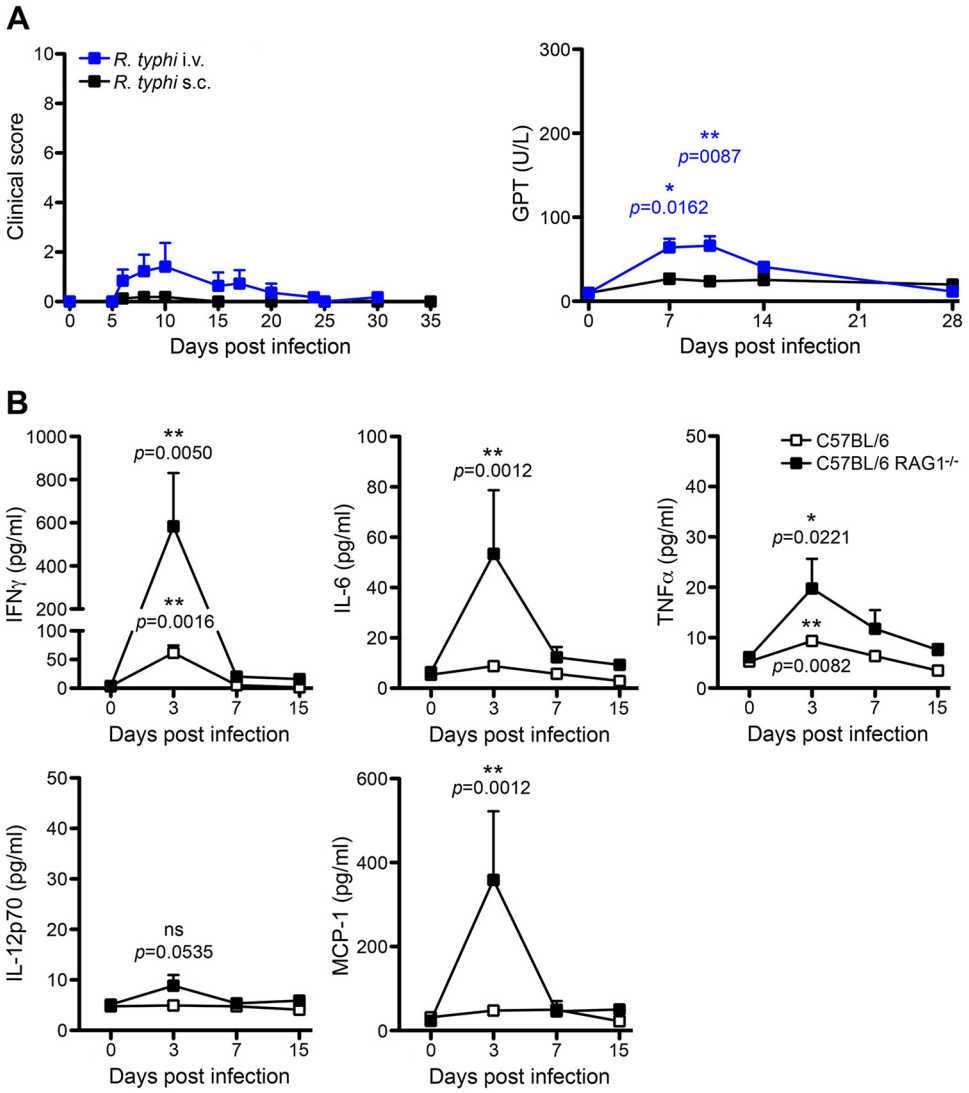

FIG 1 C57BL/6 RAG1$^{-/-}$ mice develop only mild disease and survive the initial phase of *R. typhi* infection. (A) C57BL/6 RAG1$^{-/-}$ mice were infected with 2×10^6 SFU *R. typhi* either i.v. ($n = 13$) or s.c. ($n = 16$). The course of disease was evaluated by clinical scoring (left, *y* axis) and quantification of serum GPT levels (right, *y* axis) at the indicated points in time postinfection (*x* axis). All mice survived. (B) C57BL/6 wild-type (open symbols, $n = 5$ to 7) and C57BL/6 RAG1$^{-/-}$ mice (black symbols, $n = 5$ to 7) were infected with 2×10^6 SFU *R. typhi* s.c., and plasma cytokine levels (*y* axes) were quantified with the bead-based LEGENDplex assay at the indicated points in time postinfection (*x* axes). Serum levels of IFN-γ, IL-6, TNF-α, IL-12p70, and MCP-1 are depicted. Combined results from two independent experiments are shown. Error bars show standard error of the mean (SEM). Statistical analysis was performed with the two-tailed Mann-Whitney U test. Asterisks indicate statistically significant differences compared to naive mice (day 0) (*, $P < 0.05$; **, $P < 0.01$).

turer's protocol. Amounts of 12.5 μl of plasma from EDTA blood samples were used diluted 1:2 in assay buffer.

Statistical analysis. Statistical analysis was performed with GraphPad Prism 5 software (GraphPad Software, Inc., La Jolla, CA). Student's *t* test, the Mann-Whitney U test, or two-way ANOVA followed by the Tukey test were performed as indicated in the figure legends.

RESULTS

C57BL/6 RAG1$^{-/-}$ mice survive the initial phase of *R. typhi* infection. T and B cell-deficient C57BL/6 RAG1$^{-/-}$ mice (26) have been shown to be highly resistant to infection with spotted fever group (SFG) rickettsiae, e.g., *R. conorii* (27). To analyze whether C57BL/6 RAG1$^{-/-}$ mice are more susceptible to *R. typhi* (typhus group [TG]) than to *R. conorii*, which belongs to the phylogenetically different SFG rickettsiae, we infected C57BL/6 RAG1$^{-/-}$ mice either s.c. or i.v. and followed the course of infection by *R. typhi*-specific qPCR, clinical scoring, and quantification of glutamate pyruvate transaminase (GPT) serum levels as a measure of liver damage. Similar to the observations described for the infection with SFG rickettsiae, C57BL/6 wild-type mice, as well as C57BL/6 RAG1$^{-/-}$ mice, did not develop any signs of illness and had no detectable bacterial load in various organs (data not shown), indicating early and quick elimination of *R. typhi* by innate immune mechanisms. Only C57BL/6 RAG1$^{-/-}$ mice that were infected with *R. typhi* i.v. showed temporary and mild symptoms of disease, as indicated by a low clinical score (Fig. 1A, left). Mild disease was also reflected by slightly elevated GPT serum levels, indicating mild liver damage (Fig. 1A, right). Here, GPT levels peaked on day 7 and normalized until day 14. In the end, all

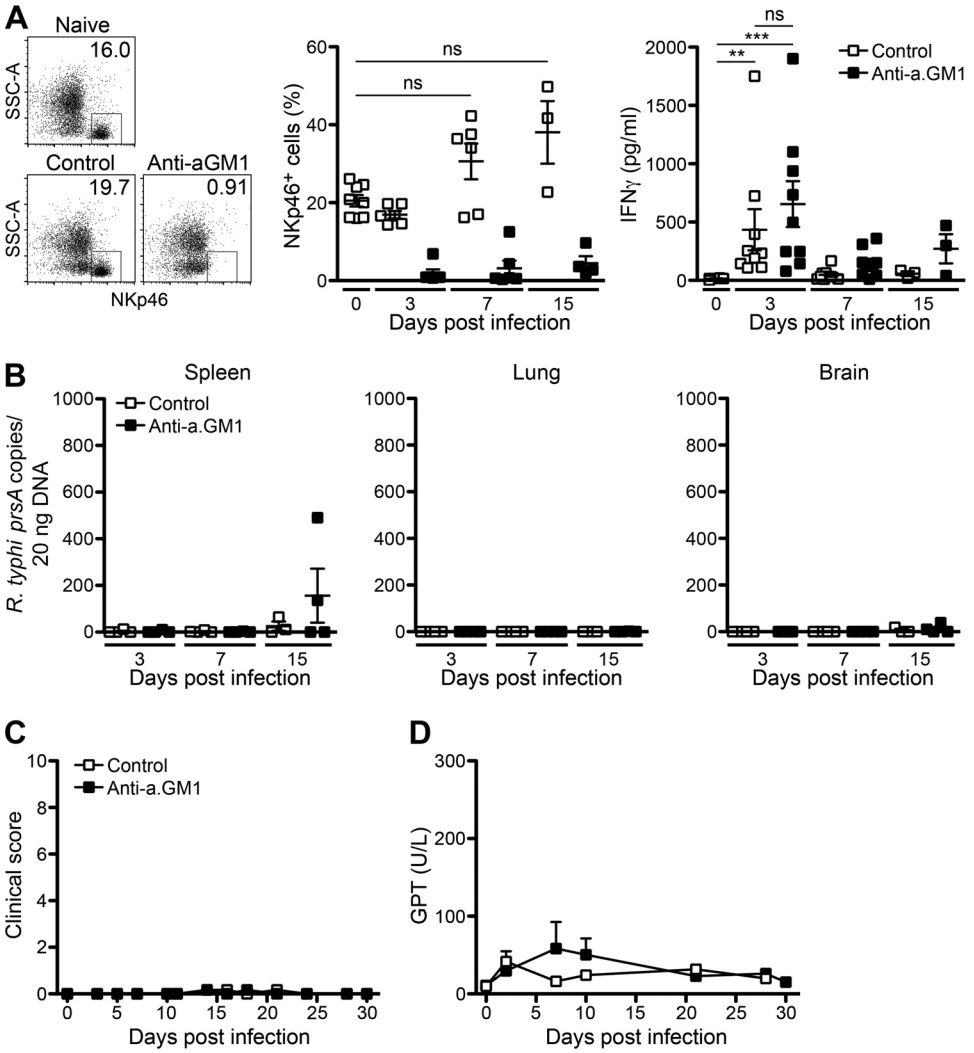

FIG 2 Depletion of NK cells does not affect the course of disease in C57BL/6 RAG1$^{-/-}$ mice upon *R. typhi* infection. (A) C57BL/6 RAG1$^{-/-}$ mice were treated with anti-asialo GM1 antibody (Anti-a.GM1) or control serum every 5 days starting 1 day prior to infection with 2×10^6 SFU *R. typhi* s.c. The percentages of NKp46$^+$ NK cells in blood and plasma levels of IFN-γ were assessed by LEGENDplex assay. Representative results for the staining of blood cells from a naive mouse and *R. typhi*-infected mice that received either control serum or anti-asialo GM1 antibody are shown in the scatter plots (day 3 postinfection). Graphs show statistical analysis of the percentages of NKp46$^+$ cells (*y* axis) and IFN-γ plasma levels (*y* axis) at indicated points in time postinfection (*x* axis). Each symbol represents the result for a single mouse; bars and whiskers show the mean and SEM. Statistical analysis was performed with the Kruskal-Wallis test. Asterisks indicate statistically significant differences (**, $P < 0.01$; ***, $P < 0.001$). SSC, side scatter. (B) Bacterial loads were determined by qPCR of *prsA* in spleen, lung, and brain tissues. *R. typhi prsA* copy numbers (*y* axis) at indicated points in time (*x* axis) are depicted. Each symbol represents the result for a single mouse. (C and D) The course of disease was evaluated by clinical scoring ($n = 5$ for each group) (*y* axis) (C) and quantification of GPT in the serum ($n = 3$ for each group) (*y* axis) (D) at the indicated points in time (*x* axes). Error bars show SEM.

mice recovered and survived independent of the route of *R. typhi* infection, indicating that innate immune mechanisms are sufficient to control *R. typhi* in the C57BL/6 strain.

IFN-γ dominates early systemic inflammatory response to *R. typhi* in C57BL/6 mice. To assess the immune response against *R. typhi* during the course of infection, we next analyzed the plasma cytokine profiles of s.c.-infected C57BL/6 wild-type and C57BL/6 RAG1$^{-/-}$ mice. Cytokines were quantified in plasma samples from days 3, 7, and 15 postinfection by employing the bead-based LEGENDplex assay. C57BL/6 RAG1$^{-/-}$ mice but not C57BL/6 wild-type mice produced significantly enhanced amounts of monocyte chemoattractant protein 1 (MCP-1)/CCL2 exclusively on day 3 postinfection (358.563.1 ± 163.842 pg/ml, versus 23.107 ± 1.880 pg/ml in PBS-treated control mice) (Fig. 1B). In addition, very low although significantly enhanced levels of systemic interleukin-6 (IL-6) and tumor necrosis factor alpha (TNF-α) were detectable in C57BL/6 RAG1$^{-/-}$ mice. Here, IL-6 was detectable only on day 3 postinfection, while low levels of TNF-α were still present on day 7 (Fig. 1B). Both cytokines were virtually absent in C57BL/6 wild-type mice. IFN-γ was clearly the dominant cytokine in both C57BL/6 wild-type and C57BL/6 RAG1$^{-/-}$ mice. It was released by C57BL/6 RAG1$^{-/-}$ and C57BL/6 wild-type mice exclusively on day 3 postinfection and, thus, clearly preceded the onset of adaptive immunity. However, significantly higher levels of IFN-γ were observed in C57BL/6 RAG1$^{-/-}$ mice (583.1 ± 247.4 pg/ml) than in C57BL/6 wild-type mice (61.88 ± 12,59 pg/ml). IFN-γ was no

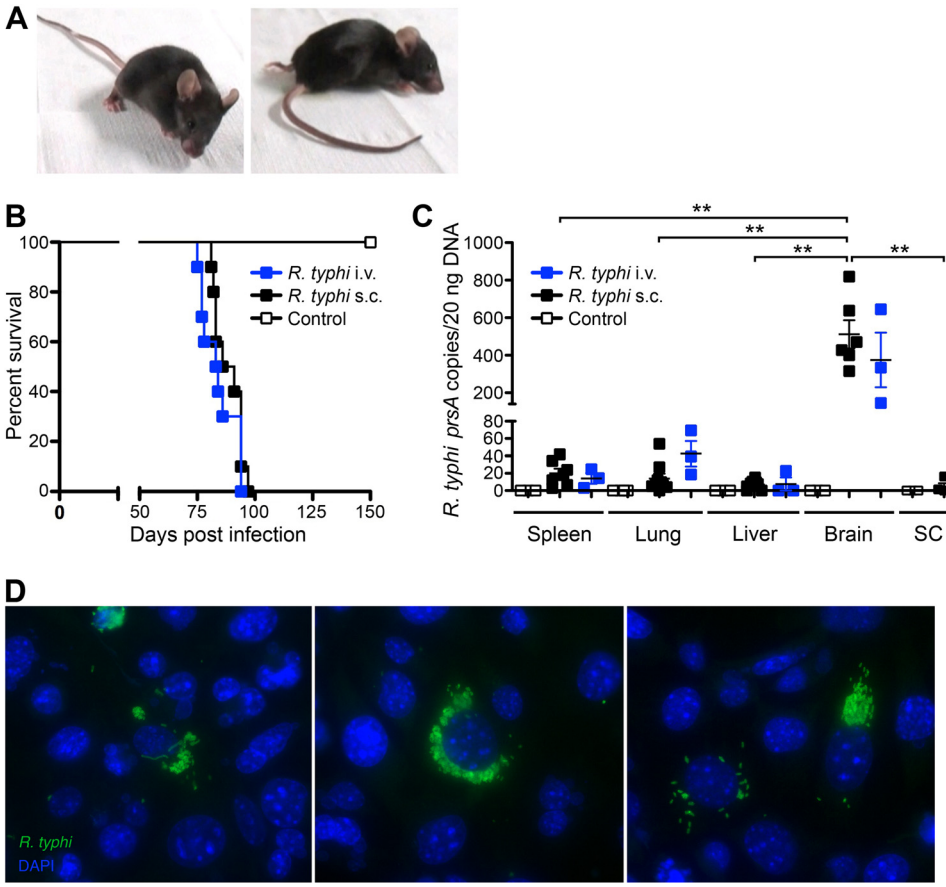

FIG 3 *R. typhi*-infected C57BL/6 RAG1$^{-/-}$ mice develop lethal neurological disorders and bacteria are present in the brain 3 to 4 months postinfection. C57BL/6 RAG1$^{-/-}$ mice were infected with 2×10^6 SFU *R. typhi* either i.v. ($n = 10$) or s.c. ($n = 10$). Control mice received PBS i.v. instead ($n = 10$). Beyond day 80, *R. typhi*-infected mice developed neurological disorders, often beginning with stroke-like symptoms and resulting in lethal paralysis. (A) Photographs of two representative mice in the early phase (left) and late phase (right) of disease are shown. (B) The percentage of survival (*y* axis) was assessed for each group at the indicated points in time postinfection (*x* axis). (C) At the time of death, bacterial loads (*y* axis) of *R. typhi*-infected C57BL/6 RAG1$^{-/-}$ mice that had been infected either i.v. or s.c. were assessed in the indicated organs by qPCR (*x* axis). SC, spinal cord. Each symbol represents the result for a single mouse. Statistical analysis was performed with the Kruskal-Wallis test. Bars and whiskers show the mean and SEM. Asterisks indicate statistically significant differences (**, $P < 0.01$). (D) Brains from two mice that were infected with *R. typhi* s.c. were isolated at the time of death and lysed. Lysates were used to inoculate L929 cells. Cells were incubated for 5 days, and supernatants of these cultures were then used to inoculate L929 cells seeded into chamber slides. Three days later, cells were stained for *R. typhi* with serum from a patient, anti-human IgG–FITC, and FITC–Alexa Fluor 488-conjugated antibody (green). Nuclei were stained with DAPI (blue).

longer detectable on day 7 in either group (Fig. 1B). Surprisingly, IL-12p70, which is considered the main IFN-γ-inducing cytokine for NK cells and T cells (30), was not significantly increased in C57BL/6 RAG1$^{-/-}$ mice at any point in time (Fig. 1B). Collectively, these data demonstrate an early and temporary inflammatory immune response which is terminated within the first 7 days after *R. typhi* infection in both C57BL/6 wild-type and C57BL/6 RAG1$^{-/-}$ mice.

Early IFN-γ may be produced by NK cells, which have been implicated in innate host defense against *R. conorii* (27) and *R. typhi* in C57BL6 RAG1$^{-/-}$ mice (20, 31). To demonstrate a potential protective role of NK cells against *R. typhi*, we depleted NK cells in C57BL/6 RAG1$^{-/-}$ mice by repeated application of anti-asialo GM1 antibody. Treatment with anti-asialo GM1 antibody almost completely eliminated NK cells from the blood for at least 3 days (Fig. 2A) and was repeated every 5 days. On day 3 postinfection, however, IFN-γ was still detectable at comparable amounts in NK cell-depleted mice and control mice (Fig. 2A). Furthermore, the absence of NK cells did not lead to detectable bacterial loads in lung and brain. Only the spleens of 2 out of 4 NK cell-depleted mice showed the presence of bacteria on day 15 postinfection (Fig. 2B). None of the animals, however, developed symptomatic disease (Fig. 2C). In addition, GPT serum levels, used as an indicator for liver damage, were not significantly enhanced (Fig. 2D). In the end, all NK cell-depleted mice ($n = 5$) survived the infection until day 30 (data not shown). These results indicate rapid bacterial clearance and protection against *R. typhi* by innate immune mechanisms independent of NK cells in mice of the C57BL/6 strain lacking T and B cells.

Reappearance of *R. typhi* in the CNS of C57BL/6 RAG1$^{-/-}$ mice induces lethal CNS inflammation months after infection. Our results presented above, as well as the observations described in the literature (20, 27), indicate that rickettsial infections, including *R. typhi*, can be controlled and cleared by the efficient innate immune response of C57BL/6 mice in the absence of T and B cells. For the first time, we here followed *R. typhi*-infected C57BL/6 RAG1$^{-/-}$ mice for several months. Surprisingly, *R. typhi*-infected mice suddenly developed neurological disorders 3 to

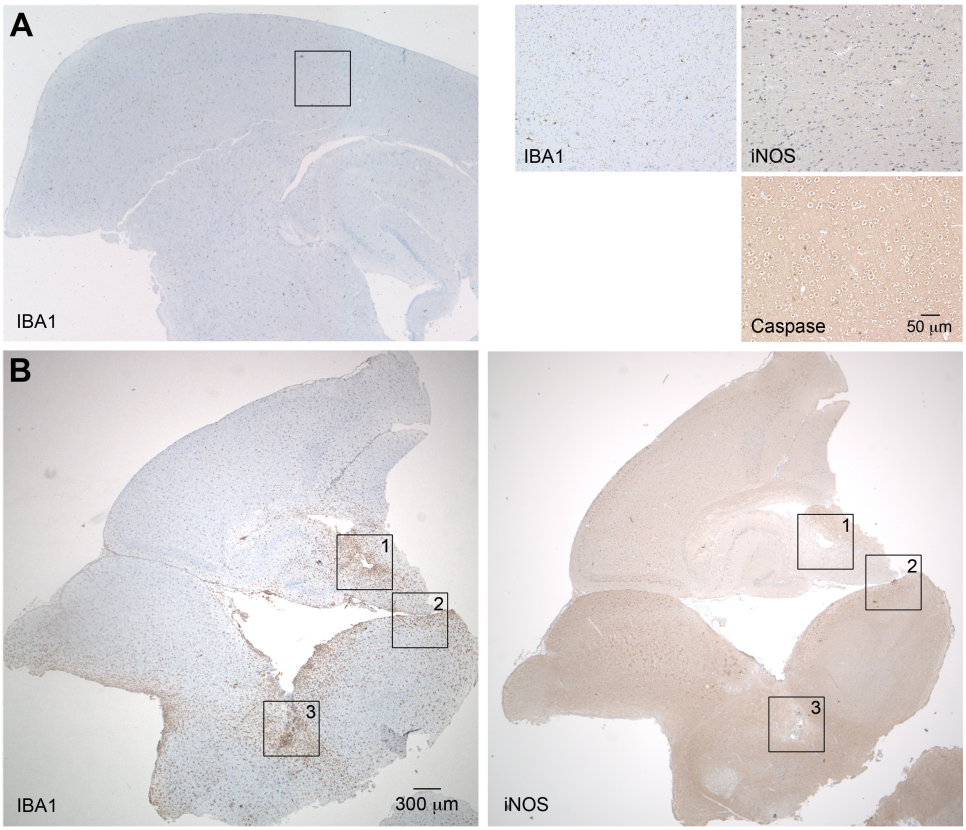

FIG 4 Accumulation of IBA1$^+$ cells in the brains of C57BL/6 RAG1$^{-/-}$ mice. (A and B) Sagittal brain sections taken from a PBS-treated C57BL/6 RAG1$^{-/-}$ control mouse (A) and a C57BL/6 RAG1$^{-/-}$ mouse previously infected with 2×10^6 SFU *R. typhi* (B) at the time of death were stained for IBA1, a marker for microglia and macrophages, as well as iNOS and caspase 3, as indicated. Overview pictures were taken at 2-fold magnification. The three panels at the top right show IBA1, iNOS, and caspase 3 staining of the brain of the control mouse at 20-fold magnification. (B) The numbered boxed areas in the brain sections of the *R. typhi*-infected mouse were analyzed by further staining, images of which are shown in Fig. 5 and discussed in its legend.

4 months after infection. The majority of the mice showed stroke-like symptoms in the beginning of disease, e.g., the head hanging to one side, tremor, or unsteadiness. Thereafter, the severity of symptoms rapidly progressed within 5 to 7 days, resulting in ataxia, paralysis, and/or dramatic weight loss. Figure 3A shows representative photographs of a mouse in the early (left) and late (right) phases of disease. Video S1 in the supplemental material presents three mice at different stages of disease. Essentially, 100% of the *R. typhi*-infected C57BL/6 RAG1$^{-/-}$ mice died between day 80 and day 120 independently of the route of infection (Fig. 3B), while control mice that received PBS were healthy. Interestingly, at the time of death, high numbers of *R. typhi* were detectable by qPCR, predominantly in the brains of the animals, whereas other organs, such as the spleen, liver, and lung, were hardly affected. On average, 20 ng of organ DNA contained 19.93 ± 5.402 *R. typhi prsA* copies in the spleen, 13.96 ± 5.606 copies in the lung, and 6.356 ± 2.455 copies in the liver, while 511.8 ± 75.32 copies were detectable in the brain. In addition, only small amounts of *R. typhi* were detectable in the spinal cord (4.588 ± 3.932 copies per 20 ng DNA) (Fig. 3C).

To further demonstrate the presence of living bacteria in the brain, we inoculated L929 cells with lysates from homogenized brains taken from two *R. typhi*-infected mice at the time of death. Both cultures were highly infected after 5 days of incubation. The bacteria were detectable by qPCR in large amounts (data not shown). In addition, *R. typhi* was detected by immunofluorescent staining in the cytosol of L929 cells seeded in chamber slides and inoculated with supernatant from these cultures. Clusters of proliferating bacteria were visible in the cytosol, while some cells also showed filamentous arrangements of *R. typhi* (Fig. 3D). These data demonstrate that living bacteria are present in the brain of *R. typhi*-infected C57BL/6 RAG1$^{-/-}$ mice.

To gain insight into the processes in the brain, we further produced sagittal sections of brains taken from *R. typhi*-infected C57BL/6 RAG1$^{-/-}$ mice at the time of death. Serial sections were stained for *R. typhi*, iNOS, active caspase 3 as a marker for apoptotic cell death, the granulocyte marker Ly-6G, and IBA1 (ionized calcium binding adapter molecule 1). IBA1 was used as it is exclusively expressed by macrophages and, in the brain, by microglia. In addition, IBA1 is upregulated in microglia following nerve injury and activation (32), as well as in macrophages and neutrophils in response to IFN-γ (33). Figure 4 shows an overview of IBA1 staining of the brain from a PBS-treated C57BL/6 RAG1$^{-/-}$ control mouse (Fig. 4A) at 2-fold magnification (left) and staining for IBA1, iNOS, and caspase 3 at 20-fold magnification (right). In the healthy brain, IBA1-positive (IBA1$^+$) microglia were equally distributed in the parenchyma and showed a ramified morphology that is characteristic of inactive microglia. As expected, iNOS$^+$ and caspase 3$^+$ cells were not detectable in the brains of control mice. In contrast to healthy brains, the brains of *R. typhi*-infected

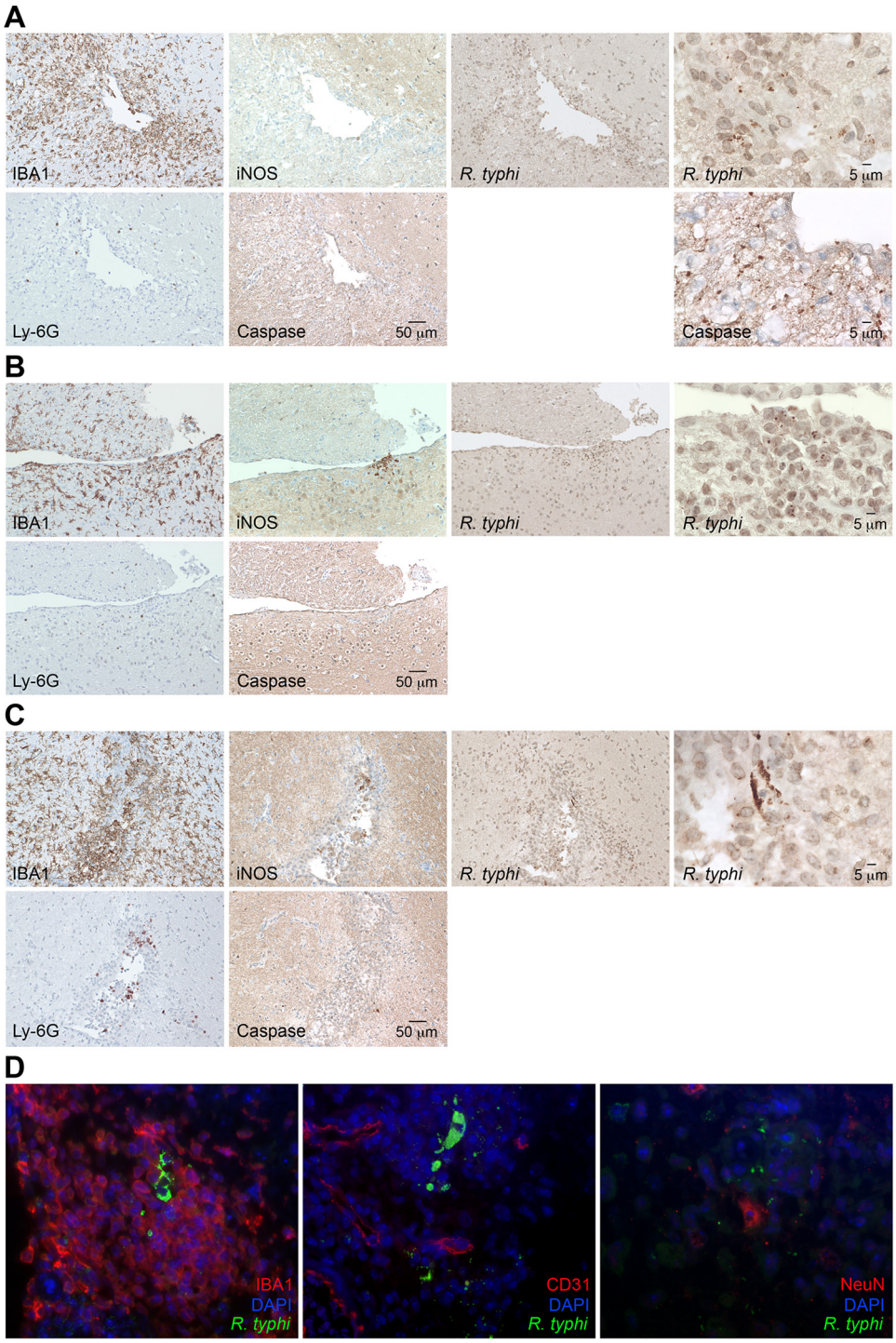

FIG 5 Detection of *R. typhi* particles and IBA1$^+$, Ly-6G$^+$, CD31$^+$, NeuN$^+$, apoptotic, and iNOS-expressing cells. (A to C) The three numbered boxed areas in the brain sections of the *R. typhi*-infected mouse shown in Fig. 4 were further stained for IBA1, iNOS, and caspase 3, as well as for *R. typhi*, employing human patient serum. Stained serial sections are shown for area 1 (A), area 2 (B), and area 3 (C) of Fig. 4B. (D) *R. typhi* was further detected in brain sections by immunofluorescent staining with serum from a human patient (green). In addition, sections were stained for IBA1, CD31 (endothelial cells), or NeuN (neurons) (red). Nuclei were stained with DAPI (blue).

C57BL/6 RAG1$^{-/-}$ mice at the time of death showed a massive accumulation of IBA1$^+$ cells all over the brain which was already visible at 2-fold magnification (Fig. 4B). In some areas (Fig. 4B, areas 1, 2, and 3), iNOS-expressing cells were observed. Figure 5 shows images of the boxed areas in Fig. 4 with further staining for Ly-6G, iNOS, caspase 3, and *R. typhi* at 20-fold and 100-fold magnification. *R. typhi* particles were detectable in all three areas (Fig. 5A to C). In area 1 (Fig. 5A), the majority of IBA1$^+$ cells morpho-

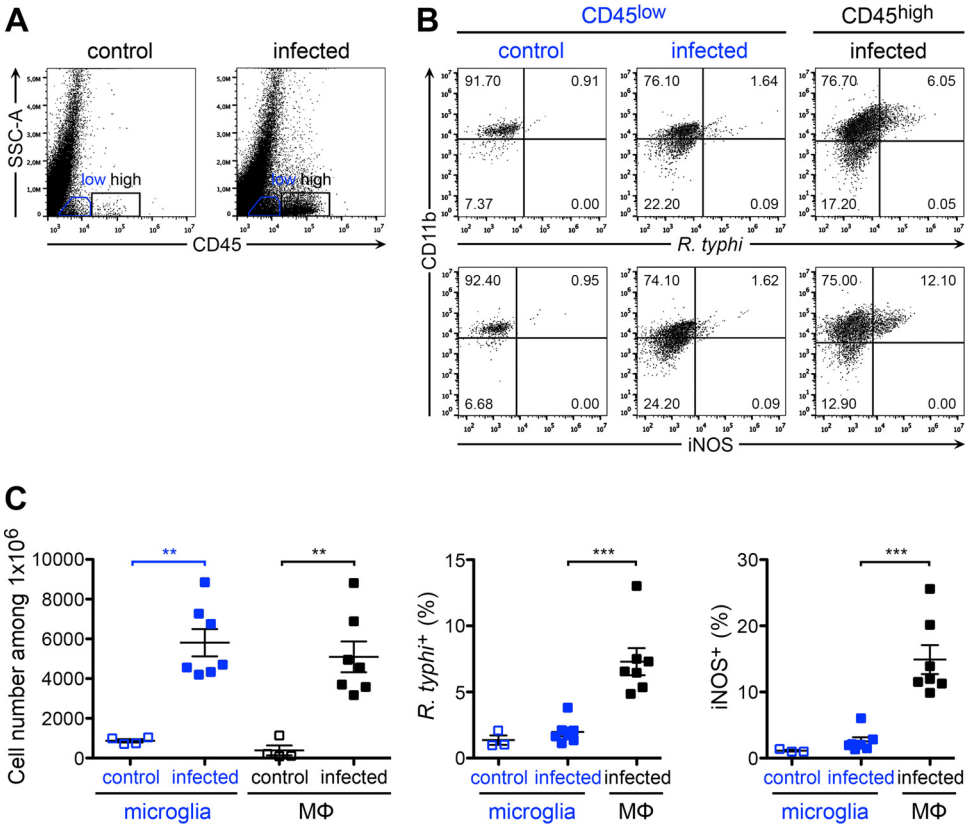

FIG 6 Expansion of microglia and infiltration of *R. typhi*-harboring inflammatory macrophages. (A) C57BL/6 RAG1$^{-/-}$ mice were infected with 2×10^6 SFU *R. typhi* s.c. At the time of death, brain cells were stained for CD45 (*x* axis) and gated on CD45^{low} (blue gate) and infiltrating CD45^{high} cells (black gate) for further analysis. Representative results of staining for CD45 on brain cells from a control C57BL/6 RAG1$^{-/-}$ mouse that received PBS and an *R. typhi*-infected C57BL/6 RAG1$^{-/-}$ mouse are depicted in the scatter plots. (B) Cells were further stained for CD11b (*y* axis), *R. typhi* (top, *x* axis), and iNOS (bottom, *x* axis). Representative results for brain cells gated on the CD45^{low} and CD45^{high} population from a control and an *R. typhi*-infected C57BL/6 RAG1$^{-/-}$ mouse are shown. (C) CD45^{low} CD11b$^+$ cells were defined as microglia and CD45^{high} CD11b$^+$ as infiltrating macrophages (MΦ). Total numbers (*y* axis) of microglia and MΦ were assessed in the brains of control and *R. typhi*-infected C57BL/6 RAG1$^{-/-}$ mice, as indicated on the *x* axis (left). The percentages of *R. typhi*$^+$ cells (middle, *y* axis) and iNOS$^+$ cells (right, *y* axis) were determined among both populations, as indicated on the *x* axis. Each symbol represents the result for a single mouse. Combined results from two independent experiments are shown; bars and whiskers show the mean and SEM. Statistical analysis was performed with the Kruskal-Wallis test. Asterisks indicate statistically significant differences (**, $P < 0.01$; ***, $P < 0.001$).

logically resembled activated microglia rather than infiltrating macrophages. Apart from IBA1$^+$ cells, few Ly-6G$^+$ granulocytes were also detectable. In addition, the presence of caspase 3$^+$ apoptotic bodies indicated neuronal cell death in this area. Surprisingly, IBA1$^+$ cells in area 1 did not express detectable amounts of iNOS (Fig. 5A), which is usually associated with microglia-mediated neuronal damage (34, 35), as well as with bactericidal activity (36, 37). In contrast to area 1, iNOS-expressing cells were observed in areas 2 (Fig. 5B) and 3 (Fig. 5C). Here, IBA1$^+$ cells morphologically resembled infiltrating macrophages rather than microglia. In addition, a few infiltrating Ly-6G$^+$ granulocytes were also detectable. Interestingly, despite iNOS expression (Fig. 4B, right, and 5B and C), caspase 3$^+$ apoptotic cells were absent in these areas (Fig. 5B and C). The brains were further stained for IBA1, CD31 as a marker for endothelial cells, and NeuN, which is exclusively expressed in neuronal nuclei (38), in addition to *R. typhi* for immunofluorescent detection. Surprisingly, *R. typhi* was not detectable in CD31$^+$ endothelial cells and was also absent in NeuN$^+$ neurons but was exclusively found in accumulating IBA1$^+$ cells, most likely infiltrating macrophages (Fig. 5D).

Next, we further elucidated the activation status of microglia and infiltrating macrophages and performed flow cytometric analysis of cells from the brains taken from *R. typhi*-infected C57BL/6 RAG1$^{-/-}$ mice at the time of death. To discriminate resident microglia and infiltrating macrophages, the cells were stained for CD11b, a commonly used surface marker for both cell populations (39, 40), and for CD45, which is expressed at lower levels on the surface of microglia than on other immune cells (39, 41–43). According to this staining protocol, we defined microglia as CD45^{low} CD11b$^+$ cells and infiltrating macrophages as CD45^{high} CD11b$^+$ and further stained for intracellular *R. typhi* and iNOS. The results depicted in Fig. 6 show that both cell populations were significantly increased in the brains of *R. typhi*-infected mice compared to their levels in control mice (Fig. 6A and C, left), demonstrating microglial expansion and macrophage infiltration. Interestingly, *R. typhi* was detectable exclusively in CD45^{high} CD11b$^+$ infiltrating macrophages and not in CD45^{low} CD11b$^+$ microglia. Moreover, only CD45^{high} CD11b$^+$ macrophages expressed iNOS and, thus, showed an inflammatory phenotype and bactericidal activity (Fig. 6B and C). In line with the qPCR results, which revealed only small amounts of bacteria in other organs than the brain, *R. typhi* was not detectable in the

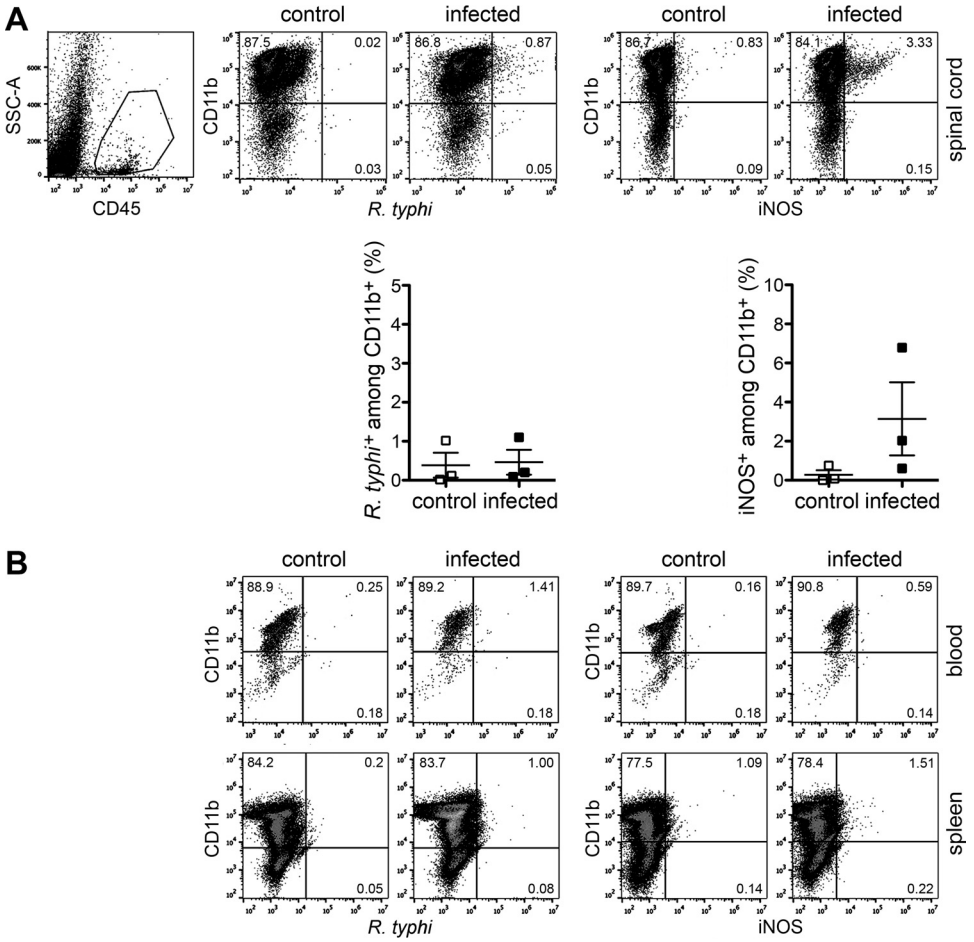

FIG 7 Inflammatory macrophages are not detectable in the periphery. (A) Cells from the spinal cords of the same control and *R. typhi*-infected C57BL/6 RAG1$^{-/-}$ mice described in the legend to Fig. 6, taken at the time of death, were gated on CD45^{+} cells and further stained for CD11b, *R. typhi*, and iNOS as indicated (scatter plots). The graphs show the statistical analysis of these measurements. Each symbol represents the result for a single mouse; bars and whiskers show the mean and SEM. (B) In a similar manner, blood and spleen cells (as indicated on the right) from the same mice were stained for CD11b, *R. typhi* (left), and iNOS (iNOS). Representative results of staining for one mouse are depicted.

spinal cord or in the blood or spleen by flow cytometry. In addition, iNOS-expressing inflammatory macrophages were not observed in the periphery. In the spinal cord, however, low numbers of iNOS-expressing macrophages were detectable in some mice (Fig. 7). These results demonstrate that *R. typhi*-induced inflammation is restricted to the CNS in C57BL/6 RAG1$^{-/-}$ mice and that *R. typhi* resides in macrophages.

Inflammatory response and neuronal cell loss in the spinal cord. Although the bacteria were hardly detectable in the spinal cord by qPCR, we observed iNOS-expressing macrophages in this part of the CNS. Therefore, we performed histological staining of the lumbar spinal cord. Compared to the results for control mice that received PBS instead of *R. typhi*, we also observed a massive accumulation of IBA1^{+} cells in the spinal cord (Fig. 8A and B). These cells were found in the gray as well as in the white matter, most likely representing microglia with a contracted activated phenotype. Some of these cells appeared to cluster around neurons. In addition, focal accumulations of infiltrating IBA1^{+} cells were detectable in *R. typhi*-infected mice in peripheral regions of the spinal cord in the pia mater and subarachnoid space. Only in these areas and not in the gray and white matter were there also iNOS-expressing IBA1^{+} cells, as well as *R. typhi* bacteria, detectable (Fig. 8A and B). As observed in the brain, the bacteria were found in infiltrating IBA1^{+} macrophages but not in CD31^{+} endothelial cells as detected by immunofluorescent stainings (Fig. 8B).

We finally asked whether *R. typhi* infection would lead to neuronal damage in the spinal cord. Therefore, we further stained the spinal cords of control mice that had been treated with PBS and *R. typhi*-infected mice for neurons with an antibody against NeuN. This staining revealed significant neuronal cell loss in *R. typhi*-infected C57BL/6 RAG1$^{-/-}$ mice in the ventral horn and to some extent also in the dorsal horn (Fig. 9), clearly demonstrating neuronal damage.

***R. typhi* infection leads to temporary brain inflammation in C57BL/6 wild-type mice.** Having shown that *R. typhi* persists in immunocompromised mice, causing severe CNS inflammation, we next asked whether the brains of C57BL/6 wild-type mice might also be affected by *R. typhi* infection. To that end, C57BL/6 mice were infected with *R. typhi* i.v. and sagittal brain sections were taken 8 days postinfection to perform histological staining for T cells (CD3), macrophages/microglia (IBA1), iNOS, and *R.*

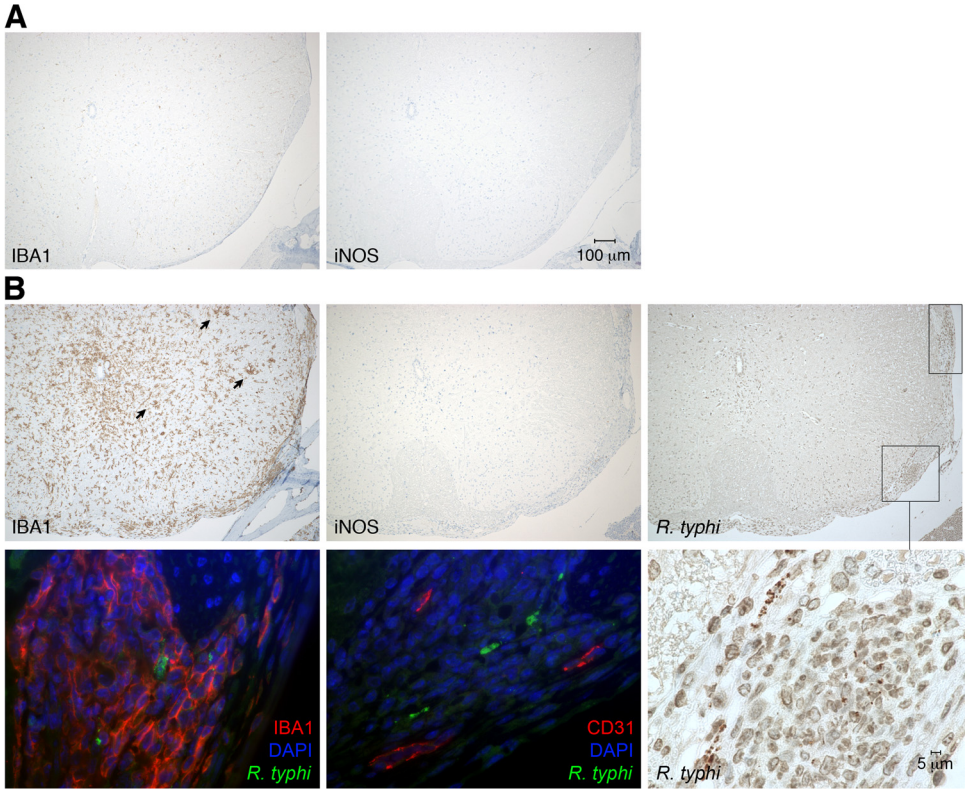

FIG 8 Detection of *R. typhi*, IBA1$^+$, CD31$^+$, and iNOS-expressing cells in the spinal cord. (A and B) Sections of spinal cords from control mice that received PBS (A) and *R. typhi*-infected C57BL/6 RAG1$^{-/-}$ mice (B) at the time of death were stained for IBA1, iNOS, and *R. typhi*. For immunofluorescent detection, sections of spinal cords from *R. typhi*-infected C57BL/6 RAG1$^{-/-}$ mice were stained for either IBA1 or CD31 (red), in addition to *R. typhi* (green) and DAPI (blue). Representative spinal cord sections from a group of five mice are depicted. Arrows indicate accumulating IBA1$^+$ cells in association with neurons.

typhi. Figure 10 shows overview photographs at 2-fold magnification. Here, several foci of accumulating IBA1$^+$ cells in the parenchyma of the brains of *R. typhi*-infected C57BL/6 wild-type mice were obvious (Fig. 10A). Twentyfold magnifications of the relevant areas (Fig. 10A, boxed areas 1 and 2) are depicted in Fig. 10B and C, respectively. Generally, intact *R. typhi* particles were no longer detectable at this time. However, IBA1$^+$ cells and CD3$^+$ T cells had accumulated around blood vessels where *R. typhi* antigen was present (Fig. 10B). Furthermore, infiltrating IBA1$^+$ cells and CD3$^+$ T cells were observed in the brain parenchyma where *R. typhi* antigen was also detectable (Fig. 10C), indicating the previous presence of the bacteria. IBA1$^+$ cells in the brains of *R. typhi*-infected C57BL/6 wild-type mice generally did not express iNOS and, thus, did not show characteristics of inflammatory microglia/

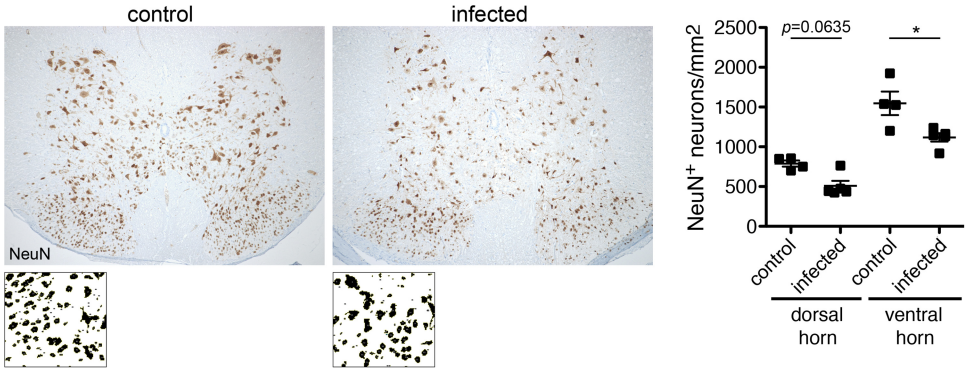

FIG 9 Neuronal cell loss in the spinal cords of *R. typhi*-infected C57BL/6 RAG1$^{-/-}$ mice. Sections of the spinal cords from control mice that received PBS and *R. typhi*-infected C57BL/6 RAG1$^{-/-}$ mice at the time of death were stained for NeuN. Representative sections of the spinal cords from a control and an *R. typhi*-infected mouse are shown. NeuN$^+$ neurons were counted with ImageJ software, creating binary pictures as shown below. The graph shows statistical analysis of NeuN$^+$ neurons per mm^2 (*y* axis) in the ventral and dorsal horns of the spinal cord. Each symbol represents the result for a single mouse; bars and whiskers show mean and SEM. Statistical analysis was performed with the Mann-Whitney U test. Asterisks indicate statistically significant differences (*, $P < 0.05$).

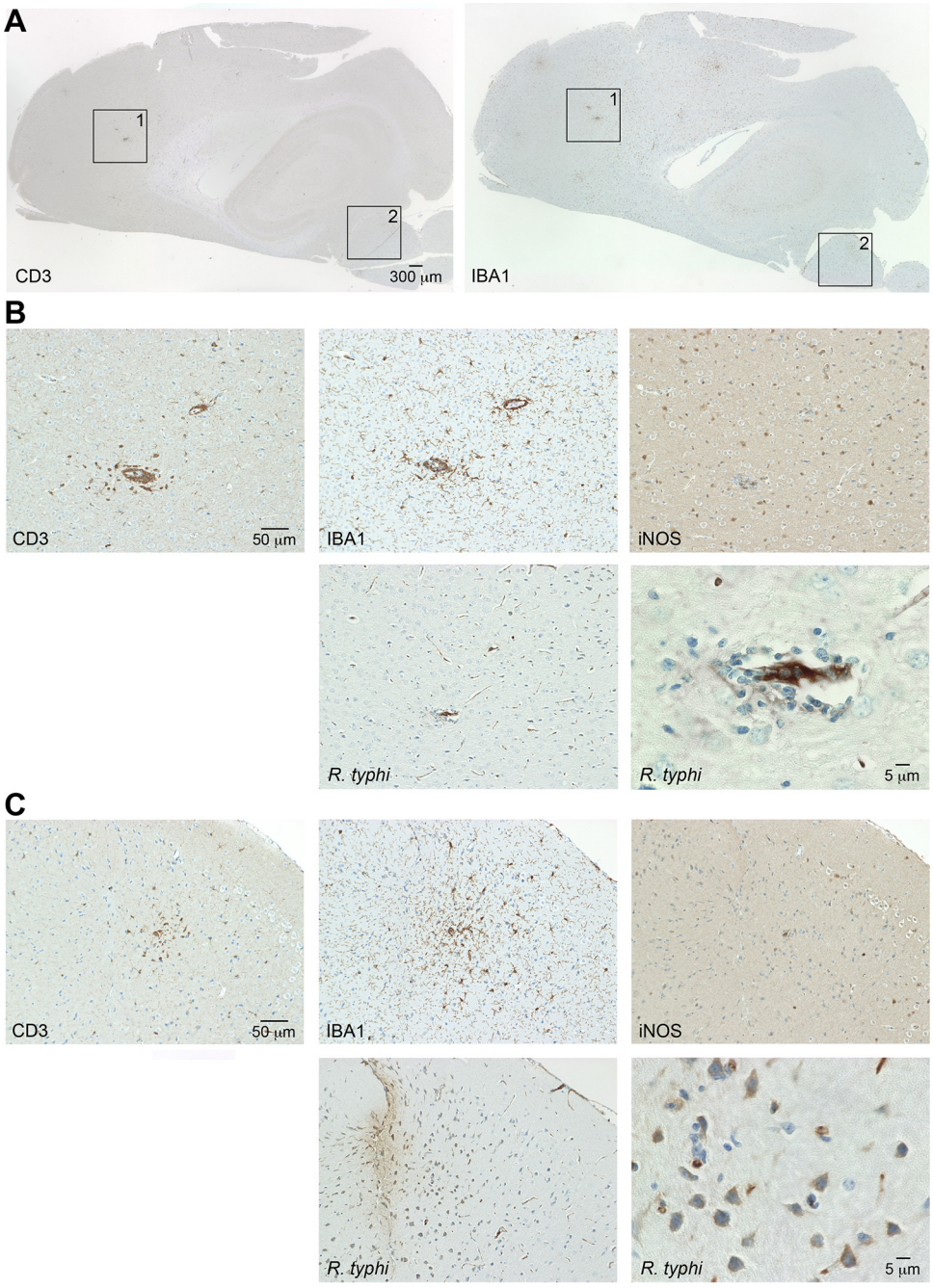

FIG 10 Cellular infiltrates and detection of *R. typhi* in the brains of C57BL/6 wild-type mice in the initial phase of infection. (A) C57BL/6 wild-type mice were infected with 2×10^6 SFU *R. typhi* i.v. Brain sections were prepared on day 8 postinfection and stained for IBA1 and CD3, as indicated. (B and C) The numbered boxed areas in panel A were further analyzed by staining of serial sections for IBA1, CD3, iNOS, and *R. typhi*, employing anti-*R. typhi* antibody (clone BNI52). (B) Area 1; (C) area 2.

macrophages (Fig. 10B and C). These data demonstrate that *R. typhi* enters the brain of C57BL/6 wild-type mice, leading to temporary focal T cell and macrophage infiltration.

***R. typhi* persists in C57BL/6 and BALB/c wild-type mice.** The results presented so far show that *R. typhi* infection affects the brain of C57BL/6 wild-type mice and persists in immunocompromised C57BL/6 RAG1$^{-/-}$ mice, causing lethal CNS inflammation after months of latency. At present, *R. prowazekii*, the closest relative of *R. typhi*, is the only rickettsial bacterium that is known to persist, and it can cause the so-called Brill-Zinsser disease years to decades after primary infection (44–47). Therefore, we finally asked whether wild-type mice are indeed capable of completely eliminating *R. typhi*. To clarify this question, we analyzed different organs from wild-type mice by immunofocus assay, as described in Materials and Methods and shown in Fig. 11A. In this assay, small amounts of bacteria that may be present in different organs

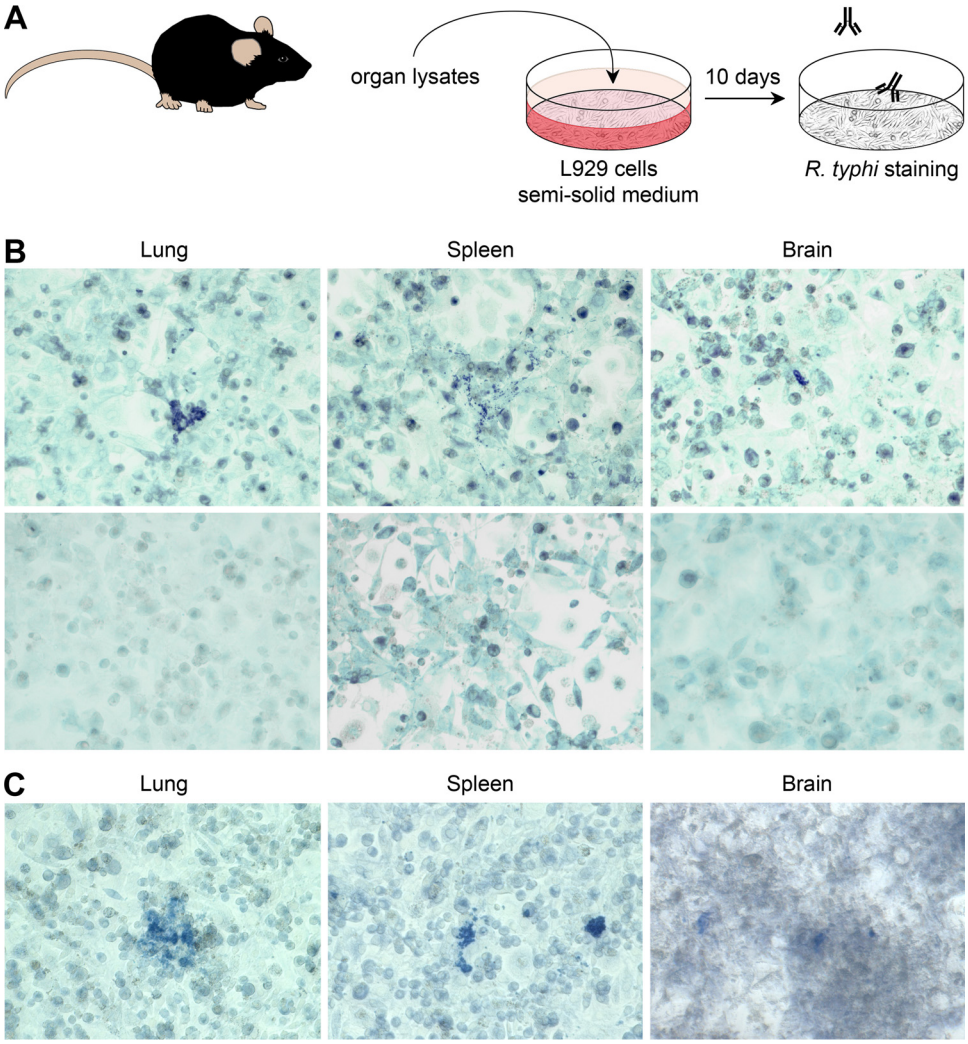

FIG 11 *R. typhi* persists in the lungs, spleens, and brains of resistant C57BL/6 and BALB/c wild-type mice. (A) Persistence of *R. typhi* was analyzed by immunofocus assay as schematically depicted. Organs from infected mice 6 to 12 months postinfection were smashed and cultured with irradiated L929 cells in semisolid medium. *R. typhi* was detected 8 to 10 days later by staining with anti-*R. typhi* antibody (clone BNI52). (B) Top, representative spots of *R. typhi*-containing cells after culture of L929 cells with lysates from lung, spleen, and brain from a C57BL/6 mouse 1 year after s.c. infection with 2×10^6 SFU *R. typhi* are shown. Bottom, organs from a naive mouse were used as a control. (C) In the same manner, organs taken from a BALB/c mouse 6 months after s.c. infection with 2×10^6 SFU *R. typhi* were analyzed. The results are representative for two mice for each experiment.

but are not detectable by qPCR or other direct methods grow in cell cultures inoculated with organ lysates and overlaid with semisolid medium. After 8 to 10 days, the bacteria become detectable as spots of infected cells if they have been replicating. Employing this assay, we show that *R. typhi* can be reisolated from the lung, spleen, and brain of infected C57BL/6 mice even 1 year after infection (Fig. 11B) in the absence of any immunosuppression. In a second approach, we used BALB/c mice, which have also been described as being resistant to *R. typhi* infection (18, 19). Again, *R. typhi* could be recultivated from the same organs 6 months after infection (Fig. 11C).

For the first time, these results provide clear evidence that *R. typhi* persists in immunocompetent hosts and can be reisolated from different organs.

DISCUSSION

This is the first report demonstrating persistence of *R. typhi* in different organs and different immunocompetent mouse strains (BALB/c and C57BL/6) that are considered to be resistant to this infection. Moreover, *R. typhi* can be controlled for several months by innate immune mechanisms in mice of the C57BL/6 strain, while adaptive immunity is required to permanently prevent recrudescence. In C57BL/6 RAG1$^{-/-}$ mice where adaptive immunity is missing, *R. typhi* shows a clear neurotropism and reappears months after primary infection, predominantly in the CNS. This reappearance of *R. typhi* is associated with severe CNS inflammation and neuronal cell loss, resulting in lethal paralysis. Because control mice that received the buffer instead of *R. typhi* remained healthy, we conclude that reappearing *R. typhi* bacteria are responsible for the CNS inflammation and disease.

In contrast to C3H/eN mice, which have been described as being susceptible to rickettsial infections, other mouse strains, such as BALB/c and C57BL/6, are normally resistant (17, 20, 21). The resistance of C57BL/6 mice to rickettsial infections is in part ascribed to the robust innate immune response of this strain, as

C57BL/6 RAG1$^{-/-}$ mice that lack adaptive immunity have been shown to clear and survive infection with *R. conorii* until day 20 (27). In line with these observations, C57BL/6 RAG1$^{-/-}$ mice developed only mild disease and survived *R. typhi* infection not only for 20 days but for several months. The mechanisms mediating control of *R. typhi* for such a long period of time are completely unclear. In the case of *R. conorii* infection, it has been demonstrated that IFN-γ plays an important role in protection, as neutralization of this cytokine resulted in fatal disease (22). We observed enhanced systemic IFN-γ release very early on day 3 after *R. typhi* infection in C57BL/6 wild-type and C57BL/6 RAG1$^{-/-}$ mice, while the cytokine was no longer detectable on day 7. Thus, this response clearly preceded the adaptive immune response.

In *R. conorii*-infected C3H/HeN mice, increased NK cell activity has been observed very early on day 2 postinfection. Moreover, depletion of NK cells enhanced the susceptibility of C3H/HeN mice to *R. conorii* infection (20), indicating the involvement of NK cells in protection. In contrast, depletion of NK cells in C57BL/6 RAG1$^{-/-}$ mice did not result in significantly enhanced bacterial load or symptomatic disease upon *R. typhi* infection, and all mice survived. Thus, NK cells might not be essential for the control of *R. typhi* in C57BL/6 RAG1$^{-/-}$ mice, while other cells, such as macrophages, may play a dominant role. The observation that susceptible C3H/HeN mice show delayed activation of macrophages compared to the time of macrophage activation in resistant BALB/c mice upon *Orientia tsutsugamushi* infection *in vivo* (48) indicates the involvement of these cells in protection against rickettsial infections. Moreover, early IFN-γ expression that was observed on day 3 after *R. typhi* infection did not derive from NK cells, indicating other cellular sources of this cytokine. These may include macrophages, which are generally capable of producing IFN-γ (49, 50) and release this cytokine in response to infection with intracellular pathogens, such as *Mycobacterium tuberculosis*, although in small amounts (51–53). Furthermore, cytokines like IL-12 and IL-18 can induce IFN-γ production in macrophages (54, 55), and IL-12 synergizes with intracellular bacteria, such as mycobacteria, in the induction of IFN-γ in *in vitro*-infected macrophages (53). Finally, IFN-γ induces its own expression in macrophages (56). Cytokines other than IFN-γ that were detectable in the plasma of *R. typhi*-infected C57BL/6 RAG1$^{-/-}$ mice were IL-6 and TNF-α, as well as the chemokine MCP-1/CCL2. IL-6 and TNF-α are mainly produced by macrophages and dendritic cells (DCs) (57–61). In addition, monocytes/macrophages also represent the major cellular source for MCP-1/CCL2 (62, 63), suggesting a strong contribution of these cells to the early response against *R. typhi*.

In infected C57BL/6 RAG1$^{-/-}$ mice, *R. typhi* predominantly reappeared in the brain, and this was independent of the infection route. How *R. typhi* enters the brain, however, is not clear. It has been shown that *R. conorii* passes the blood-brain barrier if administered systemically by i.v. injection (64). Generally, direct invasion via endothelial cell infection is considered to be the main mechanism by which intracellular bacteria that target endothelial cells, such as rickettsiae and *Listeria monocytogenes*, enter the brain (65). Our observation that T cells and macrophages accumulate around blood vessels in the brain of C57BL/6 wild-type mice after i.v. challenge with *R. typhi* may also argue for this hypothesis. In addition to endothelial cell damage that is mediated by the bacteria themselves, inflammatory cytokines (TNF-α, IL-1β, and IFN-γ) that are induced to protect against rickettsial infections have been demonstrated to contribute to enhanced microvascular permeability and, thus, could facilitate bacterial entry (66). This is in part mediated by the induction of NO production in endothelial cells (67–70). However, another mechanism for CNS invasion is via infected phagocytes. It has, for example, been shown that *L. monocytogenes* parasitizes circulating phagocytes and that these can establish CNS infection and induce meningoencephalitis even under antibiotic treatment (71). Such "shuttle" service has also been demonstrated for viruses, such as simian immunodeficiency virus (SIV) in a macaque model of neuropathogenic human immunodeficiency virus (HIV) (72), and is discussed for *O. tsutsugamushi* (65). With regard to the infection of C57BL/6 RAG1$^{-/-}$ mice with *R. typhi*, the following different scenarios are conceivable. (i) *R. typhi* enters the brain in the initial phase of infection via damaged endothelial cells. In the brain, the bacteria can then be controlled for a relatively long period of time, perhaps with the help of NK cells, or the bacteria achieve a dormant status or latency before growing again. (ii) Alternatively, *R. typhi* persists in the periphery and enters the brain via parasitized phagocytes, similarly to *L. monocytogenes*. This could be a mechanism to evade efficient protective immune mechanisms that are active in the periphery but missing in the special immune situation in the brain.

At present, we cannot answer the question of which scenario of persistence is true. We observed infiltrating CD45^{high} CD11b^{+} macrophages that, in contrast to microglia, contained *R. typhi* and expressed iNOS in the brain and spinal cord. Moreover, intact *R. typhi* particles were detectable in the areas of macrophage infiltration by histological staining, indicating bacterial replication and incapability of these cells to kill *R. typhi*. In line with these findings, *R. typhi* has been shown to survive and to replicate in murine and human macrophages (73, 74), which is also true for other rickettsiae, such as *O. tsutsugamushi* (18, 19) and *Rickettsia akari* (75). Therefore, it is not clear whether these cells are recruited to the CNS for defense against *R. typhi* by phagocytosis and killing of intracellular particles or whether they may serve as a kind of shuttle. The observation that *R. typhi* was not detectable in endothelial cells but exclusively in infiltrating macrophages may be taken as a hint that these cells are capable of shuttling *R. typhi* into the CNS. These *R. typhi*-harboring cells mainly appeared at the ventricle borders in the brain and in the pia mater and subarachnoid space in the spinal cord, indicating bacterial distribution via the liquor that is produced in the ventricles and maintained in the subarachnoid space. On the other hand, immune responses take place in the brain already in the initial phase of infection. Together with the fact that *R. typhi* can be recultivated from the brain of wild-type mice months after infection, this indicates that *R. typhi* also enters the brain at early points in time and persists at low numbers in this organ. The fact that *R. typhi* was not detectable in the brain of C57BL/6 RAG1$^{-/-}$ mice by qPCR before day 70 postinfection (data not shown), however, indicates a sudden expansion of *R. typhi* rather than continuous bacterial growth.

Microglia and astrocytes are considered to act in concert as the intrinsic immune system of the CNS (76). Microglia share many characteristics with macrophages and are key players in the initiation of the inflammatory response (77). Similarly to peripheral macrophages, they can be activated by various stimuli, including the recognition of microbes by Toll-like receptors (TLR) like TLR4 and proinflammatory cytokines like IFN-γ (37). Microglia

act as phagocytes and acquire cytotoxic function upon activation. This is usually associated with the production of inflammatory cytokines and iNOS-mediated NO production (36, 37). In the brain, as well as the spinal cord, of C57BL/6 RAG1$^{-/-}$ mice, we observed massive expansion and accumulation of CD45^{low} CD11b^{+} and IBA1^{+} microglia. In the brain, apoptotic bodies were detectable in the areas of microglial accumulation, indicating neuronal cell death. Moreover, clusters of microglia were observed in association with neurons in the spinal cord, where neuronal cell loss was clearly detectable. In CNS infections and inflammatory and degenerative CNS diseases, microglia have been implicated in neuronal apoptosis, which is strongly associated with NO release (34, 35). Microglia in *R. typhi* infection, however, did not express iNOS and, thus, did not acquire bactericidal function. Furthermore, they did not harbor *R. typhi*, suggesting that these cells do not directly recognize and act against *R. typhi*. Apart from mediating inflammatory responses, microglia also function as sensor cells that detect abnormalities in the brain and migrate to a site of injury to exert neuroprotective and neurotrophic functions (78). This activity has been associated with a non-classically activated phenotype (79–84) that these cells may also achieve in *R. typhi* infection. If this is true, it is unclear how neuronal cell death is then induced. One possible explanation is that *R. typhi* directly infects neuronal cells. It has been shown that *R. rickettsii* efficiently infects neurons, causing neuronal apoptosis (85). If this is true for *R. typhi*, the bacterium might not be directly accessible for microglia but could induce neuronal damage, leading to the recruitment of neuroprotective microglia. However, *R. typhi* was not detectable in neuronal cells in the brain or spinal cord, where the bacteria did not appear in the gray matter at all. In addition, bacterial content was generally low in the spinal cord. These findings argue against direct infection of neurons by *R. typhi* and strongly suggest that neuronal damage is an immunopathological effect mediated by activated microglia by yet-unknown mechanisms rather than by the bacteria themselves.

In wild-type mice, T cells, especially CD8^{+} cytotoxic T cells that can directly attack infected cells, are mainly responsible for protection against infections with intracellular pathogens, such as the rickettsiae (86). Cytotoxic activity of CD8^{+} T cells, together with IFN-γ production, has been demonstrated to be essential for protection against SFG rickettsiae (22–25). Moreover, T cells have been shown to confer cross-protection between SFG and TG rickettsiae in susceptible C3H/HeN mice (87). In line with these observations, immunocompetent C57BL/6 wild-type mice are capable of controlling *R. typhi*. Nevertheless, we demonstrate for the first time that *R. typhi* persists in different organs, including the spleen, lung, and brain, in these mice. Our results suggest that *R. typhi* may also persist in humans, possibly dependent on the immune status of a patient. So far, *R. prowazekii*, the closest relative of *R. typhi* and causative agent of epidemic typhus, is the only rickettsial bacterium that is known to persist latently in humans and to reappear years to decades after the primary infection, causing the so-called Brill-Zinsser disease. Meningitis and neurological symptoms, including stupor, confusion, delirium, and coma, are common in epidemic typhus (88, 89), as well as in Brill-Zinsser disease (44–47). It is suggested that stress or waning immunity can reactivate *R. prowazekii* (90); e.g., corticosteroids, such as dexamethasone, can trigger the recurrence of *R. prowazekii* in mice (91). This may also be true for *R. typhi*, although recurrence of *R. typhi* in humans has not been described as yet. Reactivation of *R. prowazekii* can occur irrespective of antibiotic treatment. Mice treated with doxycycline during primary infection with *R. prowazekii* developed rickettsemia after the administration of dexamethasone, although at lower levels than mice that had not been treated with doxycycline (91). Thus, the risk of reappearance of rickettsiae may depend on proper timing of antibiotic therapy during primary infection.

The observation that *R. typhi* reappears predominantly in the CNS of C57BL/6 RAG1$^{-/-}$ mice and can also be found in the brain of *R. typhi*-infected wild-type mice demonstrates a neurotropism for *R. typhi*. In line with these findings, several cases of meningitis and encephalitis in *R. typhi* patients have been reported (92–96). In some cases, delayed or prolonged neurologic manifestations have been observed (92, 94). Moreover, *R. typhi* was found to be an important cause of CNS infections in Laos, where endemic typhus is common (97). Furthermore, it has been demonstrated that the CNS is affected in MSF caused by *R. conorii* (98) and in the late phase of RMSF caused by *R. rickettsii* (4, 99) and other rickettsial infections (100). Symptoms include ataxia, paresis, and paralysis (100) and resemble those observed in *R. typhi*-infected C57BL/6 RAG1$^{-/-}$ mice.

Collectively, our data demonstrate for the first time a neurotropism and the persistence of *R. typhi*, suggesting that these bacteria should be taken under consideration in cases of undifferentiated CNS inflammatory diseases, especially in low-income countries where *R. typhi* is common.

ACKNOWLEDGMENTS

We thank Susanne Krasemann and Kristin Hartmann from the Mouse Pathology Service at the University Medical Center Hamburg-Eppendorf, Hamburg, Germany.

REFERENCES

1. **Sekeyova Z, Roux V, Raoult D.** 2001. Phylogeny of Rickettsia spp. inferred by comparing sequences of 'gene D', which encodes an intracytoplasmic protein. Int J Syst Evol Microbiol **51:**1353–1360. http://dx.doi.org/10.1099/00207713-51-4-1353.
2. **Mansueto P, Vitale G, Cascio A, Seidita A, Pepe I, Carroccio A, di Rosa S, Rini GB, Cillari E, Walker DH.** 2012. New insight into immunity and immunopathology of Rickettsial diseases. Clin Dev Immunol **2012:**967852. http://dx.doi.org/10.1155/2012/967852.
3. **Azad AF, Beard CB.** 1998. Rickettsial pathogens and their arthropod vectors. Emerg Infect Dis **4:**179–186. http://dx.doi.org/10.3201/eid0402.980205.
4. **Walker D, Raoult D, Dumler JS, Marrie T (ed).** 2008. Rickettsial diseases. McGraw-Hill, New York, NY.
5. **Dupont HT, Brouqui P, Faugere B, Raoult D.** 1995. Prevalence of antibodies to Coxiella burnetii, Rickettsia conorii, and Rickettsia typhi in seven African countries. Clin Infect Dis **21:**1126–1133. http://dx.doi.org/10.1093/clinids/21.5.1126.
6. **Parola P, Miller RS, McDaniel P, Telford SR, III, Rolain JM, Wongsrichanalai C, Raoult D.** 2003. Emerging rickettsioses of the Thai-Myanmar border. Emerg Infect Dis **9:**592–595. http://dx.doi.org/10.3201/eid0905.020511.
7. **Suputtamongkol Y, Suttinont C, Niwatayakul K, Hoontrakul S, Limpaiboon R, Chierakul W, Losuwanaluk K, Saisongkork W.** 2009. Epidemiology and clinical aspects of rickettsioses in Thailand. Ann N Y Acad Sci **1166:**172–179. http://dx.doi.org/10.1111/j.1749-6632.2009.04514.x.
8. **Phongmany S, Rolain JM, Phetsouvanh R, Blacksell SD, Soukkhaseum V, Rasachack B, Phiasakha K, Soukkhaseum S, Frichithavong K, Chu V, Keolouangkhot V, Martinez-Aussel B, Chang K, Darasavath C, Rattanavong O, Sisouphone S, Mayxay M, Vidamaly S, Parola P, Thammavong C, Heuangvongsy M, Syhavong B, Raoult D, White NJ, Newton PN.** 2006. Rickettsial infections and fever,

Vientiane, Laos. Emerg Infect Dis **12:**256–262. http://dx.doi.org/10.3201/eid1202.050900.
9. **Maude RR, Maude RJ, Ghose A, Amin MR, Islam MB, Ali M, Bari MS, Majumder MI, Tanganuchitcharnchai A, Dondorp AM, Paris DH, Bailey RL, Faiz MA, Blacksell SD, Day NP.** 2014. Serosurveillance of Orientia tsutsugamushi and Rickettsia typhi in Bangladesh. Am J Trop Med Hyg **91:**580–583. http://dx.doi.org/10.4269/ajtmh.13-0570.
10. **Azad AF.** 1990. Epidemiology of murine typhus. Annu Rev Entomol **35:**553–569. http://dx.doi.org/10.1146/annurev.en.35.010190.003005.
11. **Chaniotis B, Psarulaki A, Chaliotis G, Gozalo Garcia G, Gozadinos T, Tselentis Y.** 1994. Transmission cycle of murine typhus in Greece. Ann Trop Med Parasitol **88:**645–647.
12. **Rathi N, Rathi A.** 2010. Rickettsial infections: Indian perspective. Indian Pediatr **47:**157–164. http://dx.doi.org/10.1007/s13312-010-0024-3.
13. **Kuloglu F.** 2013. Rickettsial infections. Dis Mol Med **1:**39–45. http://dx.doi.org/10.5455/dmm.20130704110837.
14. **Jensenius M, Fournier PE, Raoult D.** 2004. Rickettsioses and the international traveler. Clin Infect Dis **39:**1493–1499. http://dx.doi.org/10.1086/425365.
15. **Dill T, Dobler G, Saathoff E, Clowes P, Kroidl I, Ntinginya E, Machibya H, Maboko L, Loscher T, Hoelscher M, Heinrich N.** 2013. High seroprevalence for typhus group rickettsiae, southwestern Tanzania. Emerg Infect Dis **19:**317–320. http://dx.doi.org/10.3201/eid1902.120601.
16. **Raoult D, Woodward T, Dumler JS.** 2004. The history of epidemic typhus. Infect Dis Clin North Am **18:**127–140. http://dx.doi.org/10.1016/S0891-5520(03)00093-X.
17. **Groves MG, Osterman JV.** 1978. Host defenses in experimental scrub typhus: genetics of natural resistance to infection. Infect Immun **19:**583–588.
18. **Nacy CA, Meltzer MS.** 1979. Macrophages in resistance to rickettsial infection: macrophage activation in vitro for killing of Rickettsia tsutsugamushi. J Immunol **123:**2544–2549.
19. **Nacy CA, Groves MG.** 1981. Macrophages in resistance to rickettsial infections: early host defense mechanisms in experimental scrub typhus. Infect Immun **31:**1239–1250.
20. **Billings AN, Feng HM, Olano JP, Walker DH.** 2001. Rickettsial infection in murine models activates an early anti-rickettsial effect mediated by NK cells and associated with production of gamma interferon. Am J Trop Med Hyg **65:**52–56.
21. **Fang R, Ismail N, Soong L, Popov VL, Whitworth T, Bouyer DH, Walker DH.** 2007. Differential interaction of dendritic cells with Rickettsia conorii: impact on host susceptibility to murine spotted fever rickettsiosis. Infect Immun **75:**3112–3123. http://dx.doi.org/10.1128/IAI.00007-07.
22. **Feng HM, Popov VL, Walker DH.** 1994. Depletion of gamma interferon and tumor necrosis factor alpha in mice with Rickettsia conorii-infected endothelium: impairment of rickettsicidal nitric oxide production resulting in fatal, overwhelming rickettsial disease. Infect Immun **62:**1952–1960.
23. **Feng H, Popov VL, Yuoh G, Walker DH.** 1997. Role of T lymphocyte subsets in immunity to spotted fever group rickettsiae. J Immunol **158:**5314–5320.
24. **Walker DH, Olano JP, Feng HM.** 2001. Critical role of cytotoxic T lymphocytes in immune clearance of rickettsial infection. Infect Immun **69:**1841–1846. http://dx.doi.org/10.1128/IAI.69.3.1841-1846.2001.
25. **Valbuena G, Feng HM, Walker DH.** 2002. Mechanisms of immunity against rickettsiae. New perspectives and opportunities offered by unusual intracellular parasites. Microbes Infect **4:**625–633. http://dx.doi.org/10.1016/S1286-4579(02)01581-2.
26. **Mombaerts P, Iacomini J, Johnson RS, Herrup K, Tonegawa S, Papaioannou VE.** 1992. RAG-1-deficient mice have no mature B and T lymphocytes. Cell **68:**869–877. http://dx.doi.org/10.1016/0092-8674(92)90030-G.
27. **Fang R, Ismail N, Walker DH.** 2012. Contribution of NK cells to the innate phase of host protection against an intracellular bacterium targeting systemic endothelium. Am J Pathol **181:**185–195. http://dx.doi.org/10.1016/j.ajpath.2012.03.020.
28. **Nathan C, Xie QW.** 1994. Regulation of biosynthesis of nitric oxide. J Biol Chem **269:**13725–13728.
29. **Papp S, Richardt U, Fleischer B, Osterloh A.** 2013. A new monoclonal anti-human CD83 antibody for flow cytometry, Western blot analysis, and ELISA. Monoclon Antib Immunodiagn Immunother **32:**98–104. http://dx.doi.org/10.1089/mab.2012.0080.
30. **Trinchieri G.** 1998. Immunobiology of interleukin-12. Immunol Res **17:**269–278. http://dx.doi.org/10.1007/BF02786451.
31. **Rollwagen FM.** 1988. Role of natural killer cells in the early clearance of Rickettsia typhi in mice. Adv Exp Med Biol **239:**163–168. http://dx.doi.org/10.1007/978-1-4757-5421-6_16.
32. **Ito D, Imai Y, Ohsawa K, Nakajima K, Fukuuchi Y, Kohsaka S.** 1998. Microglia-specific localisation of a novel calcium binding protein, Iba1. Brain Res Mol Brain Res **57:**1–9. http://dx.doi.org/10.1016/S0169-328X(98)00040-0.
33. **Utans U, Arceci RJ, Yamashita Y, Russell ME.** 1995. Cloning and characterization of allograft inflammatory factor-1: a novel macrophage factor identified in rat cardiac allografts with chronic rejection. J Clin Invest **95:**2954–2962. http://dx.doi.org/10.1172/JCI118003.
34. **Brown GC.** 2007. Mechanisms of inflammatory neurodegeneration: iNOS and NADPH oxidase. Biochem Soc Trans **35:**1119–1121. http://dx.doi.org/10.1042/BST0351119.
35. **Brown GC, Neher JJ.** 2010. Inflammatory neurodegeneration and mechanisms of microglial killing of neurons. Mol Neurobiol **41:**242–247. http://dx.doi.org/10.1007/s12035-010-8105-9.
36. **MacMicking J, Xie QW, Nathan C.** 1997. Nitric oxide and macrophage function. Annu Rev Immunol **15:**323–350. http://dx.doi.org/10.1146/annurev.immunol.15.1.323.
37. **Rock RB, Gekker G, Hu S, Sheng WS, Cheeran M, Lokensgard JR, Peterson PK.** 2004. Role of microglia in central nervous system infections. Clin Microbiol Rev **17:**942–964. http://dx.doi.org/10.1128/CMR.17.4.942-964.2004.
38. **Mullen RJ, Buck CR, Smith AM.** 1992. NeuN, a neuronal specific nuclear protein in vertebrates. Development **116:**201–211.
39. **Perego C, Fumagalli S, De Simoni MG.** 2011. Temporal pattern of expression and colocalization of microglia/macrophage phenotype markers following brain ischemic injury in mice. J Neuroinflammation **8:**174. http://dx.doi.org/10.1186/1742-2094-8-174.
40. **Perego C, Fumagalli S, De Simoni MG.** 2013. Three-dimensional confocal analysis of microglia/macrophage markers of polarization in experimental brain injury. J Vis Exp **2013:**50605. http://dx.doi.org/10.3791/50605.
41. **Fumagalli S, Perego C, Ortolano F, De Simoni MG.** 2013. CX3CR1 deficiency induces an early protective inflammatory environment in ischemic mice. Glia **61:**827–842. http://dx.doi.org/10.1002/glia.22474.
42. **Gelderblom M, Leypoldt F, Steinbach K, Behrens D, Choe CU, Siler DA, Arumugam TV, Orthey E, Gerloff C, Tolosa E, Magnus T.** 2009. Temporal and spatial dynamics of cerebral immune cell accumulation in stroke. Stroke **40:**1849–1857. http://dx.doi.org/10.1161/STROKEAHA.108.534503.
43. **Gesuete R, Storini C, Fantin A, Stravalaci M, Zanier ER, Orsini F, Vietsch H, Mannesse ML, Ziere B, Gobbi M, De Simoni MG.** 2009. Recombinant C1 inhibitor in brain ischemic injury. Ann Neurol **66:**332–342. http://dx.doi.org/10.1002/ana.21740.
44. **Stein A, Purgus R, Olmer M, Raoult D.** 1999. Brill-Zinsser disease in France. Lancet **353:**1936. http://dx.doi.org/10.1016/S0140-6736(99)01995-9.
45. **Turcinov D, Kuzman I, Herendic B.** 2000. Failure of azithromycin in treatment of Brill-Zinsser disease. Antimicrob Agents Chemother **44:**1737–1738. http://dx.doi.org/10.1128/AAC.44.6.1737-1738.2000.
46. **Lutwick LI.** 2001. Brill-Zinsser disease. Lancet **357:**1198–1200. http://dx.doi.org/10.1016/S0140-6736(00)04339-7.
47. **Faucher JF, Socolovschi C, Aubry C, Chirouze C, Hustache-Mathieu L, Raoult D, Hoen B.** 2012. Brill-Zinsser disease in Moroccan man, France, 2011. Emerg Infect Dis **18:**171–172. http://dx.doi.org/10.3201/eid1801.111057.
48. **Nacy CA, Leonard EJ, Meltzer MS.** 1981. Macrophages in resistance to rickettsial infections: characterization of lymphokines that induce rickettsiacidal activity in macrophages. J Immunol **126:**204–207.
49. **Gessani S, Belardelli F.** 1998. IFN-gamma expression in macrophages and its possible biological significance. Cytokine Growth Factor Rev **9:**117–123. http://dx.doi.org/10.1016/S1359-6101(98)00007-0.
50. **Frucht DM, Fukao T, Bogdan C, Schindler H, O'Shea JJ, Koyasu S.** 2001. IFN-gamma production by antigen-presenting cells: mechanisms emerge. Trends Immunol **22:**556–560. http://dx.doi.org/10.1016/S1471-4906(01)02005-1.
51. **Fenton MJ, Vermeulen MW, Kim S, Burdick M, Strieter RM, Kornfeld**

H. 1997. Induction of gamma interferon production in human alveolar macrophages by Mycobacterium tuberculosis. Infect Immun **65:**5149–5156.
52. **Robinson CM, O'Dee D, Hamilton T, Nau GJ.** 2010. Cytokines involved in interferon-gamma production by human macrophages. J Innate Immun **2:**56–65. http://dx.doi.org/10.1159/000247156.
53. **Xing Z, Zganiacz A, Santosuosso M.** 2000. Role of IL-12 in macrophage activation during intracellular infection: IL-12 and mycobacteria synergistically release TNF-alpha and nitric oxide from macrophages via IFN-gamma induction. J Leukoc Biol **68:**897–902.
54. **Puddu P, Fantuzzi L, Borghi P, Varano B, Rainaldi G, Guillemard E, Malorni W, Nicaise P, Wolf SF, Belardelli F, Gessani S.** 1997. IL-12 induces IFN-gamma expression and secretion in mouse peritoneal macrophages. J Immunol **159:**3490–3497.
55. **Munder M, Mallo M, Eichmann K, Modolell M.** 1998. Murine macrophages secrete interferon gamma upon combined stimulation with interleukin (IL)-12 and IL-18: A novel pathway of autocrine macrophage activation. J Exp Med **187:**2103–2108. http://dx.doi.org/10.1084/jem.187.12.2103.
56. **Di Marzio P, Puddu P, Conti L, Belardelli F, Gessani S.** 1994. Interferon gamma upregulates its own gene expression in mouse peritoneal macrophages. J Exp Med **179:**1731–1736. http://dx.doi.org/10.1084/jem.179.5.1731.
57. **Trinchieri G.** 1995. Interleukin-12: a proinflammatory cytokine with immunoregulatory functions that bridge innate resistance and antigen-specific adaptive immunity. Annu Rev Immunol **13:**251–276. http://dx.doi.org/10.1146/annurev.iy.13.040195.001343.
58. **Xing Z.** 2000. Current understanding of macrophage type 1 cytokine responses during intracellular infections. Histol Histopathol **15:**199–205.
59. **Gordon S.** 2007. The macrophage: past, present and future. Eur J Immunol **37**(Suppl 1)**:**S9–S17. http://dx.doi.org/10.1002/eji.200737638.
60. **Stow JL, Low PC, Offenhauser C, Sangermani D.** 2009. Cytokine secretion in macrophages and other cells: pathways and mediators. Immunobiology **214:**601–612. http://dx.doi.org/10.1016/j.imbio.2008.11.005.
61. **Trinchieri G.** 2003. Interleukin-12 and the regulation of innate resistance and adaptive immunity. Nat Rev Immunol **3:**133–146. http://dx.doi.org/10.1038/nri1001.
62. **Yoshimura T, Robinson EA, Tanaka S, Appella E, Leonard EJ.** 1989. Purification and amino acid analysis of two human monocyte chemoattractants produced by phytohemagglutinin-stimulated human blood mononuclear leukocytes. J Immunol **142:**1956–1962.
63. **Yoshimura T, Yuhki N, Moore SK, Appella E, Lerman MI, Leonard EJ.** 1989. Human monocyte chemoattractant protein-1 (MCP-1). Full-length cDNA cloning, expression in mitogen-stimulated blood mononuclear leukocytes, and sequence similarity to mouse competence gene JE. FEBS Lett **244:**487–493.
64. **Rydkina E, Sahni SK, Santucci LA, Turpin LC, Baggs RB, Silverman DJ.** 2004. Selective modulation of antioxidant enzyme activities in host tissues during Rickettsia conorii infection. Microb Pathog **36:**293–301. http://dx.doi.org/10.1016/j.micpath.2004.01.002.
65. **Drevets DA, Leenen PJ, Greenfield RA.** 2004. Invasion of the central nervous system by intracellular bacteria. Clin Microbiol Rev **17:**323–347. http://dx.doi.org/10.1128/CMR.17.2.323-347.2004.
66. **Woods ME, Olano JP.** 2008. Host defenses to Rickettsia rickettsii infection contribute to increased microvascular permeability in human cerebral endothelial cells. J Clin Immunol **28:**174–185. http://dx.doi.org/10.1007/s10875-007-9140-9.
67. **Li H, Jerrells TR, Spitalny GL, Walker DH.** 1987. Gamma interferon as a crucial host defense against Rickettsia conorii in vivo. Infect Immun **55:**1252–1255.
68. **Jerrells TR, Li H, Walker DH.** 1988. In vivo and in vitro role of gamma interferon in immune clearance of Rickettsia species. Adv Exp Med Biol **239:**193–200. http://dx.doi.org/10.1007/978-1-4757-5421-6_19.
69. **Feng HM, Walker DH.** 1993. Interferon-gamma and tumor necrosis factor-alpha exert their antirickettsial effect via induction of synthesis of nitric oxide. Am J Pathol **143:**1016–1023.
70. **Walker DH, Popov VL, Crocquet-Valdes PA, Welsh CJ, Feng HM.** 1997. Cytokine-induced, nitric oxide-dependent, intracellular antirickettsial activity of mouse endothelial cells. Lab Invest **76:**129–138.
71. **Drevets DA, Jelinek TA, Freitag NE.** 2001. Listeria monocytogenes-infected phagocytes can initiate central nervous system infection in mice. Infect Immun **69:**1344–1350. http://dx.doi.org/10.1128/IAI.69.3.1344-1350.2001.
72. **Lane JH, Sasseville VG, Smith MO, Vogel P, Pauley DR, Heyes MP, Lackner AA.** 1996. Neuroinvasion by simian immunodeficiency virus coincides with increased numbers of perivascular macrophages/microglia and intrathecal immune activation. J Neurovirol **2:**423–432. http://dx.doi.org/10.3109/13550289609146909.
73. **Beaman L, Wisseman CL, Jr.** 1976. Mechanisms of immunity in typhus infections. VI. Differential opsonizing and neutralizing action of human typhus rickettsia-specific cytophilic antibodies in cultures of human macrophages. Infect Immun **14:**1071–1076.
74. **Radulovic S, Price PW, Beier MS, Gaywee J, Macaluso JA, Azad A.** 2002. Rickettsia-macrophage interactions: host cell responses to Rickettsia akari and Rickettsia typhi. Infect Immun **70:**2576–2582. http://dx.doi.org/10.1128/IAI.70.5.2576-2582.2002.
75. **Walker DH, Hudnall SD, Szaniawski WK, Feng HM.** 1999. Monoclonal antibody-based immunohistochemical diagnosis of rickettsialpox: the macrophage is the principal target. Mod Pathol **12:**529–533.
76. **Shrikant P, Benveniste EN.** 1996. The central nervous system as an immunocompetent organ: role of glial cells in antigen presentation. J Immunol **157:**1819–1822.
77. **Cross AK, Woodroofe MN.** 2001. Immunoregulation of microglial functional properties. Microsc Res Tech **54:**10–17. http://dx.doi.org/10.1002/jemt.1115.
78. **Luo XG, Chen SD.** 2012. The changing phenotype of microglia from homeostasis to disease. Transl Neurodegener **1:**9. http://dx.doi.org/10.1186/2047-9158-1-9.
79. **Kigerl KA, Gensel JC, Ankeny DP, Alexander JK, Donnelly DJ, Popovich PG.** 2009. Identification of two distinct macrophage subsets with divergent effects causing either neurotoxicity or regeneration in the injured mouse spinal cord. J Neurosci **29:**13435–13444. http://dx.doi.org/10.1523/JNEUROSCI.3257-09.2009.
80. **Tarassishin L, Suh HS, Lee SC.** 2011. Interferon regulatory factor 3 plays an anti-inflammatory role in microglia by activating the PI3K/Akt pathway. J Neuroinflammation **8:**187. http://dx.doi.org/10.1186/1742-2094-8-187.
81. **Zhang Z, Zhang ZY, Schittenhelm J, Wu Y, Meyermann R, Schluesener HJ.** 2011. Parenchymal accumulation of CD163+ macrophages/microglia in multiple sclerosis brains. J Neuroimmunol **237:**73–79. http://dx.doi.org/10.1016/j.jneuroim.2011.06.006.
82. **Chen Z, Jalabi W, Shpargel KB, Farabaugh KT, Dutta R, Yin X, Kidd GJ, Bergmann CC, Stohlman SA, Trapp BD.** 2012. Lipopolysaccharide-induced microglial activation and neuroprotection against experimental brain injury is independent of hematogenous TLR4. J Neurosci **32:**11706–11715. http://dx.doi.org/10.1523/JNEUROSCI.0730-12.2012.
83. **Miron VE, Boyd A, Zhao JW, Yuen TJ, Ruckh JM, Shadrach JL, van Wijngaarden P, Wagers AJ, Williams A, Franklin RJ, ffrench-Constant C.** 2013. M2 microglia and macrophages drive oligodendrocyte differentiation during CNS remyelination. Nat Neurosci **16:**1211–1218. http://dx.doi.org/10.1038/nn.3469.
84. **Stirling DP, Cummins K, Mishra M, Teo W, Yong VW, Stys P.** 2014. Toll-like receptor 2-mediated alternative activation of microglia is protective after spinal cord injury. Brain **137:**707–723. http://dx.doi.org/10.1093/brain/awt341.
85. **Joshi SG, Kovacs AD.** 2007. Rickettsia rickettsii infection causes apoptotic death of cultured cerebellar granule neurons. J Med Microbiol **56:**138–141. http://dx.doi.org/10.1099/jmm.0.46826-0.
86. **Ismail N, Olano JP, Feng HM, Walker DH.** 2002. Current status of immune mechanisms of killing of intracellular microorganisms. FEMS Microbiol Lett **207:**111–120. http://dx.doi.org/10.1111/j.1574-6968.2002.tb11038.x.
87. **Valbuena G, Jordan JM, Walker DH.** 2004. T cells mediate cross-protective immunity between spotted fever group rickettsiae and typhus group rickettsiae. J Infect Dis **190:**1221–1227. http://dx.doi.org/10.1086/423819.
88. **Marrie TJ, Raoult D.** 1992. Rickettsial infections of the central nervous system. Semin Neurol **12:**213–224. http://dx.doi.org/10.1055/s-2008-1041178.
89. **Raoult D, Roux V, Ndihokubwayo JB, Bise G, Baudon D, Marte G, Birtles R.** 1997. Jail fever (epidemic typhus) outbreak in Burundi. Emerg Infect Dis **3:**357–360. http://dx.doi.org/10.3201/eid0303.970313.
90. **Bechah Y, Capo C, Mege JL, Raoult D.** 2008. Epidemic typhus.

Lancet Infect Dis **8:**417–426. http://dx.doi.org/10.1016/S1473-3099(08)70150-6.

91. **Bechah Y, Paddock CD, Capo C, Mege JL, Raoult D.** 2010. Adipose tissue serves as a reservoir for recrudescent Rickettsia prowazekii infection in a mouse model. PLoS One **5:**e8547. http://dx.doi.org/10.1371/journal.pone.0008547.
92. **Samra Y, Shaked Y, Maier MK.** 1989. Delayed neurologic display in murine typhus. Report of two cases. Arch Intern Med **149:**949–951.
93. **Silpapojakul K, Ukkachoke C, Krisanapan S, Silpapojakul K.** 1991. Rickettsial meningitis and encephalitis. Arch Intern Med **151:**1753–1757. http://dx.doi.org/10.1001/archinte.1991.00400090051010.
94. **Masalha R, Merkin-Zaborsky H, Matar M, Zirkin HJ, Wirguin I, Herishanu YO.** 1998. Murine typhus presenting as subacute meningoencephalitis. J Neurol **245:**665–668. http://dx.doi.org/10.1007/s004150050264.
95. **Moy WL, Ooi ST.** 2015. Abducens nerve palsy and meningitis by Rickettsia typhi. Am J Trop Med Hyg **92:**620–624. http://dx.doi.org/10.4269/ajtmh.14-0559.
96. **Simon NG, Cremer PD, Graves SR.** 2011. Murine typhus returns to New South Wales: a case of isolated meningoencephalitis with raised intracranial pressure. Med J Aust **194:**652–654.
97. **Dittrich S, Rattanavong S, Lee SJ, Panyanivong P, Craig SB, Tulsiani SM, Blacksell SD, Dance DA, Dubot-Peres A, Sengduangphachanh A, Phoumin P, Paris DH, Newton PN.** 2015. Orientia, rickettsia, and leptospira pathogens as causes of CNS infections in Laos: a prospective study. Lancet Glob Health **3:**e104–e112. http://dx.doi.org/10.1016/S2214-109X(14)70289-X.
98. **Alioua Z, Bourazza A, Lamsyah H, Erragragui Y, Boudi O, Karouach K, Ghfir M, Mossedaq R, Sedrati O.** 2003. Neurological feature of Mediterranean spotted fever: a study of four cases. Rev Med Interne **24:**824–829. (In French.) http://dx.doi.org/10.1016/j.revmed.2003.08.002.
99. **Wei TY, Baumann RJ.** 1999. Acute disseminated encephalomyelitis after Rocky Mountain spotted fever. Pediatr Neurol **21:**503–505. http://dx.doi.org/10.1016/S0887-8994(99)00028-4.
100. **Bleck TP.** 1999. Central nervous system involvement in Rickettsial diseases. Neurol Clin **17:**801–812. http://dx.doi.org/10.1016/S0733-8619(05)70167-5.